DESIGN AND DEVELOPMENT OF HIGH-FREQUENCY SWITCHING AMPLIFIERS USED FOR SMART MATERIAL ACTUATORS WITH CURRENT MODE CONTROL

Jiyuan Luan

Thesis submitted to the faculty of the Virginia Polytechnic Institute and State University in partial fulfillment of the requirements for the degree of

MASTER OF SCIENCE

In

Electrical Engineering

Dr. Fred C. Lee, Chairman

Dr. Jason Lai

Dr. Guichao Hua

July 27, 1998

Blacksburg, Virginia

Keywords: Current Mode Control, Electrostrictive Actuator, Piezoelectric Actuator, Smart Material, Switching Amplifier

DESIGN AND DEVELOPMENT OF HIGH-FREQUENCY SWITCHING AMPLIFIERS USED FOR SMART MATERIAL ACTUATORS WITH CURRENT MODE CONTROL

BY

Jiyuan Luan

Fred C. Lee, Chairman

The Bradley Department of Electrical Engineering and Computer Science

ABSTRACT

This thesis presents the design and development of two switching amplifiers used to drive the so-called smart material actuators. Different from conventional circuits, a smart material actuator is ordinarily a highly capacitive load. Its capacitance is non-linear and its strain is hysteretic with respect to its electrical control signal. This actuator's reactive load property usually causes a large portion of reactive power circulating between the power amplifier and the driven actuator, thus reduces the circuit efficiency in a linear power amplifier scenario. In this thesis, a switching amplifier design based on the PWM technique is proposed to develop a highly efficient power amplifier, and peak current mode control is proposed to reduce the actuator's hysteretic behavior. Since the low frequency current loop gain tends to be low due to the circuit's capacitive load, average current mode control is further proposed to boost the low frequency current loop gain and improve the amplifier's low frequency performance. Both of the circuits have been verified by prototype design and their experimental measurement results are given.

ACKNOWLEDGEMENTS

I would like to express my sincere gratitude to my advisor, Dr. Fred C. Lee, for his support and guidance during my graduate studies at Virginia Tech. Being one of his students and a member of VPEC was a privilege that will have an enormous impact on my future career and development.

I am grateful to Dr. Jason Lai and Dr. Guichao Hua for their positive attitude, encouragement and the knowledge they passed to me. Special thanks are due to Greg Zvonar who was my partner within this research project. His enthusiastic help has been invaluable to me.

I would also like to acknowledge all of the other VPEC students and staff with whom I shared the last three years. Thank you for all your friendship and help.

Finally, I would like to thank my family, for their love, support and encouragement.

FOR MY PARENTS

AND MY FAMILY

TABLE OF CONTENTS

CHAPTER 1. INTRODUCTION 1

1.1 Background 1

1.1.1 Smart material and smart material actuators *1*

1.1.2 Piezoelectric materials and electrostrictive materials *2*

1.1.3 Smart material applications in underwater acoustic wave cancellation *5*

1.2 Design Task and Technical Challenges 7

1.3 Motivation of Research 10

1.4 Thesis Outline 18

CHAPTER 2. POWER STAGE DESIGN AND DEVELOPMENT 20

2.1 Introduction 20

2.2 Power Stage Design 21

2.2.1 Topology and operation *21*

2.2.2 Power stage design *25*

2.3 Power Stage Small Signal Modeling 29

2.4 Power Stage Experimental Results 34

CHAPTER 3. PEAK CURRENT MODE CONTROL CIRCUIT DESIGN 36

3.1 Introduction 36

3.2 Small Signal Modeling of Peak Current Mode Control 38

3.2.1 Current loop design *38*

3.2.2 Voltage loop design *40*

3.3 Peak Current Mode Control Design and Experiment Results 41

CHAPTER 4. AVERAGE CURRENT MODE CONTROL DESIGN 47

4.1 Introduction 47

4.2 Small Signal Modeling of Average Current Mode Control 49

4.2.1 Current loop design *49*

4.2.2 Voltage loop design *55*

4.3 Average Current Mode Control Design and Experiment Results 55

CHAPTER 5. CONCLUSIONS 64

REFERENCES 66

APPENDIX A 69

VITA 71

LIST OF FIGURES

Figure 1.1 Sketch of a Smart Material Piston 6

Figure 1.2 Block Diagram of Smart Materials Used for Sonar Wave Cancellation 7

Figure 1.3 Sketch of an Electrostrictive Stack Actuator 8

Figure 1.4 Electrostrictive Material Actuator Capacitance vs. Its DC Bias Voltage 9

Figure 1.5 Input and Output Signal Relationship of the Power Amplifier 9

Figure 1.6 Frequency Response Requirement of the Power Amplifier 10

Figure 1.7 A Simplified Schematic of a Linear Power Amplifier 11

Figure 1.8 Block Diagram of Output Voltage Control Strategy 12

Figure 1.9 Non-linear Hysteretic Behaviour of Piezoelectric Materials 14

Figure 1.10 The Hysteretic Behavior of Piezoelectric Material 15

Figure 1.11 Piezoelectric Material Displacement Output Under Voltage Drive 16

Figure 1.12 Piezoelectric Material Displacement Output Under Charge Drive 16

Figure 2.1 Block Diagram of a Switching Amplifier 22

Figure 2.2 Operation of the Power Stage 23

Figure 2.3 Four Power Stages of the Switching Amplifier 24

Figure 2.4 Power Stage Small Signal Model 29

Figure 2.5 Bode Plot of Duty Cycle vs. Output Voltage 32

Figure 2.6 Bode Plot of Duty Cycle vs. Output Current 33

Figure 2.7 Power Stage Efficiency vs. Output Power 35

Figure 3.1 Principal of Peak Current Mode Control 37

Figure 3.2 Current Loop gain Using Peak Current Mode Control 39

Figure 3.3 Outer Loop Gain Simulated by Pspice Small Signal Model 42
Figure 3.4 Closed-loop Output Current to Input Reference Signal Transfer Function 43
Figure 3.5 View of a Prototype Switching Amplifier Using Peak Current Mode Control 44
Figure 3.6 View of a Prototype Switching Amplifier with Smart Material Actuators Mounted on Top of the Amplifier 44
Figure 3.7 Output Voltage and Current Waveform at 500 Hz 46
Figure 3.8 Output Voltage and Current Waveform at 10 kHz 46
Figure 4.1 Principal of Average Current Mode Control 49
Figure 4.2 Small Signal Model of Average Current Mode Control 50
Figure 4.3 Current Loop Gain of Average Current Mode Control 52
Figure 4.4 Output current to Input Signal Transfer Function Using Average Current 54
Figure 4.5 Outer Loop Gain Using Average Current Mode Control 56
Figure 4.6 Output Current to Input Signal Transfer Function 57
Figure 4.7 Output Current and Voltage Waveform at 500 Hz 58
Figure 4.8 Output Voltage and Current Waveform at 10 kHz 58
Figure 4.9 Smart Structure in Underwater Test 59
Figure 4.10 Upper View of a Surface Mounted Switching Amplifier 60
Figure 4.11 Bottom View of a Surface Mounted Switching Amplifier 60
Figure 4.12 Piezoelectric Actuator Displacement Output w/o Current Mode Control 61
Figure 4.13 Piezoelectric Actuator Displacement Output with Current Mode Control 62
Figure 4.14 Measured Sonar Wave Without Active Sonar Wave Cancellation 63
Figure 4.15 Measured Sonar Wave With Active Sonar Wave Cancellation 63

CHAPTER 1. INTRODUCTION

1.1 Background

1.1.1 Smart material and smart material actuators

The concept of smart material describes a new category of physical material having integrated sensor, actuator, power electronics and microprocessor. Smart materials are different from traditional materials because they have the potential to sense, recognize, discriminate and adjust to their environmental changes in ways that maximize their function. Introduced in the middle of the nineteen eighties, the advent of smart materials shows the effort to combine the advanced aspects of materials science with computer engineering and to create more adaptive materials with more and more complex functions for a wide variety of engineering applications [1-3].

The idea of a smart material is very interesting and novel to scientists and engineers. But there are many challenges that need to be addressed before this concept can be actually implemented. One of the challenges is the development of smart material actuators and the corresponding power electronics amplifiers, in other words, the effectors for smart materials. In the last two decades, different kinds of actuators have been investigated and explored for possible applications in the construction of smart material effectors, like actuators using conventional electromagnetic methods, actuators controlled by temperature (shape memory effect alloy), actuators made from magnetostrictive effect materials and actuators made from piezoelectric or electrostrictive materials. In general, different kinds of materials have different kinds of application environments. Among all these possible choices for actuators, piezoelectric and electrostrictive materials are considered to be especially promising because of their unique physical properties. Compared with other materials, piezoelectric and electrostrictive materials tend to have better accuracy, higher response speeds, lower power requirements, relatively higher generative forces and the possibility of miniaturization [4-5].

Since piezoelectric materials and electrostrictive materials have a lot of physical properties suitable for the application of smart material actuators, many recent studies concentrate on the development and application of these smart material actuators. Piezoelectric and electrostrictive actuators have been used in the area of noise control, active vibration cancellation, deformable mirrors, mechanical micropositioners, ultrasonic motors, piezoelectric transformers and many other applications [6-10].

1.1.2 Piezoelectric materials and electrostrictive materials

Piezoelectric materials and electrostrictive materials are two promising choices for the applications of smart material actuators because of their attractive physical properties. They both utilize the strain induced by an external electric field, a parameter that can be easily controlled. The piezoelectric effect describes the first order (linear) coupling between dielectric and elastic phenomena, and the electrostrictive effect describes the non-linear (second order or quadratic) dependence of the strain on the applied electric field. For an anisotropic, homogeneous solid, under isothermal conditions and neglecting the magnetic field effects, the components of the elastic strain tenor S_{ij} are given by the following equation [4]:

$$S_{ij} = s^{E}_{ijkl} T_{kl} + d_{ijk} E_k + M_{klij} E_k E_l + \text{higher order terms} \tag{1.1}$$

Where

T_{kl}: components of the stress tensor,

E_k, E_l: components of the electric field vectors,

s_{ijkl}^{E} : components of the elastic compliance tensor measured at constant electric field,

d_{ijk} : piezoelectric tensor define the linear electromechanical coupling, and

M_{klij} : electrostrictive coefficients defines the high order electromechanical coupling.

Usually, one material will show both linear and non-linear electromechanical coupling effects. If a composite material is designed to have large piezoelectric coefficients and small electrostrictive coefficients, the material is known as piezoelectric material; on the other hand, if a material is designed to have large electrostrictive coefficients and small piezoelectric coefficients, the material will be known as electrostrictive material.

Piezoelectric materials are the most widely used electromechanical transducer materials to date. First discovered in 1880, most piezoelectric materials can be categorized into one of the following three classes: single crystals, polymers, and poled ceramics [11]. Quartz is the classic example of the piezoelectric single crystal. PVDF, or polyvinylidine fluoride, is a typical piezoelectric polymeric material. PZT, or $Pb(Zr,Ti)O_3$, is a typical piezoelectric ceramic. Within these three categories of piezoelectric materials, PZT material represents the largest portion of the commercial market of electromechanical transducers due to its high coupling coefficients and its versatility with regard to chemical substitutions.

Piezoelectricity for a piezoelectric single crystal comes from the absence of symmetry within the crystal and this lattice structure property gives rise to a kind of spatial polarity, the “one-wayness” of the charge vector [11]. Most of the important piezoelectric materials are also ferroelectric, which results in a transformation to a high symmetry, non-piezoelectric phase

at higher temperatures. The piezoelectric effect is present only in the lower temperature phase, and the transformation temperature is known as the Curie temperature.

Non-crystal piezoelectricity was invented after the introduction of the poling process in the 1940s. Since ordinary polycrystalline materials have randomly oriented grains that will automatically cancel each other, the material will show zero net effect in natural state. The so-called poling process is a treatment that applies a strong electric field at elevated temperatures, giving the randomly oriented domain pattern a high degree of orientation, and thus resulting in a high net piezoelectric polycrystalline material.

Electrostrictive materials, on the other side, have different mechanisms than piezoelectric materials. One typical electrostrictive material is the so-called lead magnesium niobate ($Pb(Mg_{1/3}Nb_{2/3})O_3$, or PMN) material. PMN materials belong to a class of relaxor ferroelectrics [12-13], which demonstrate a strong dispersion of dielectric permittivity with frequency and display no macroscopic polarization even at temperatures well below the temperature of the maximum dielectric constant. Instead of having a well-defined Curie temperature, electrostrictive materials exhibit diffuse phase transitions throughout a Curie range due to the macrovolumes contained within the ABO_3 perovskite crystal matrix, each of which has a different local Curie temperature. The phase change of the bulk material throughout the Curie range from a cubic to an orthrombic structure generates 0.1% volume expansion of the crystal lattice upon the application of the electric field and thus generates elastic tensor.

Although electrostrictive materials like the PMN materials were introduced much later than the well-known PZT materials, many physical properties of the PMN materials like high electrostrictive strains and low-hysteretic behavior have made the PMN materials recognized as one of the most attractive materials to be used for smart material actuators [14].

1.1.3 Smart material applications in underwater acoustic wave cancellation

The concept of smart material was introduced in the middle eighties and has been applied in the fields of noise control, active vibration cancellation, deformable mirrors, mechanical micropositioners, ultrasonic motors and many of other applications. One of the newest applications for smart materials is underwater acoustic wave cancellation. Like other objects, the underwater surface of a submarine is subject to acoustic wave reflection, which makes it detectable to sonar equipment. In order to cancel the acoustic wave and to make the submarine 'invisible' to the sonar, a smart material 'sonar wave cancellation coating' is developed. This 'coating' is made from thousands of small units called pistons, and each piston is a smart material building block, which has a sensor, a digital signal processing unit, a smart material actuator array and the associated power amplifier (as shown in Figure 1.1). Each of the pistons will be individually addressable, and all of them will have the ability to sense the incoming sonar wave at their own site. To perform sonar wave cancellation, the detected local incoming signal at each piston will be sent to a local microprocessor within the piston, where the signal is combined with the information from other pistons and processed by a vibration cancellation algorithm. The local processor then generates an output sonar-wave cancellation signal to feed into the power amplifier as a command signal, where this reference signal is boosted and used to drive a smart material actuator array and finally the mechanical vibration of the smart material actuator will be used for the sonar wave cancellation(shown in Figure 1.2).

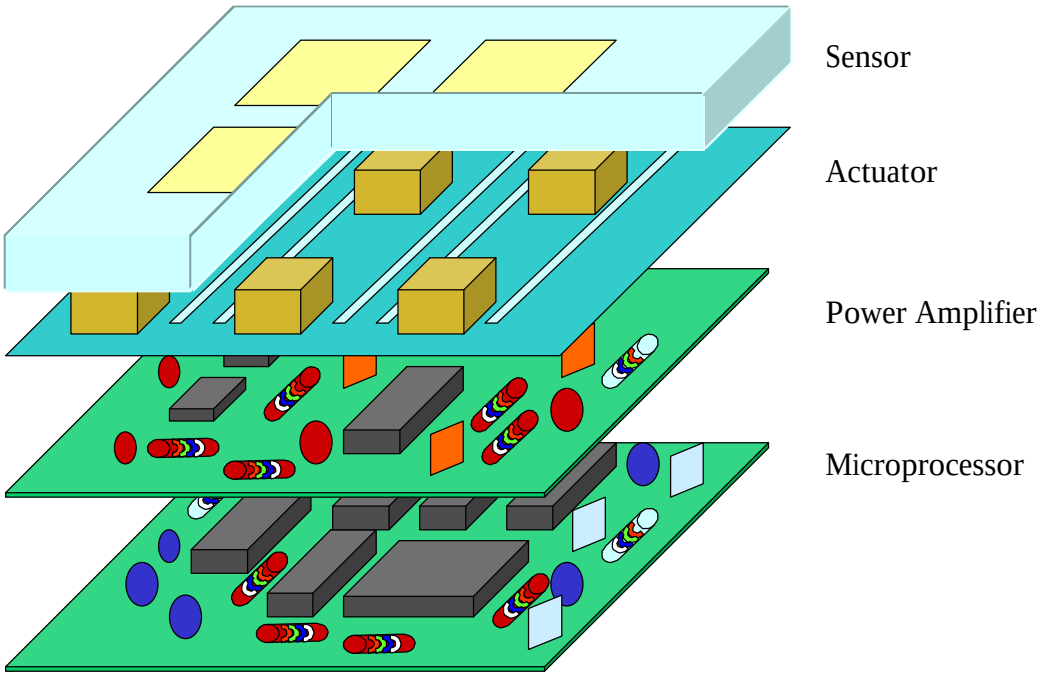

Figure 1.1 Sketch of a Smart Material Piston

Since all of the pistons will be individually addressable, each piston will have a designated power amplifier and this power amplifier has to be integrated into the corresponding piston. Limited by the physical size of the allowable application environment, the amplifier has to be high efficient and high power density.

Another critical performance requirement is the power amplifier's frequency response. As can be seen from Figure 1.2, the reference signal generated from the DSP unit needs to have minimum magnitude distortion and phase lag to create the best sonar wave cancellation effect when it gets through the power amplifier and converts to the mechanical vibration by the actuator array. This has been proved to be very difficult with conventional output voltage control strategy. The approach of current mode control strategy is proposed and investigated to resolve this problem.

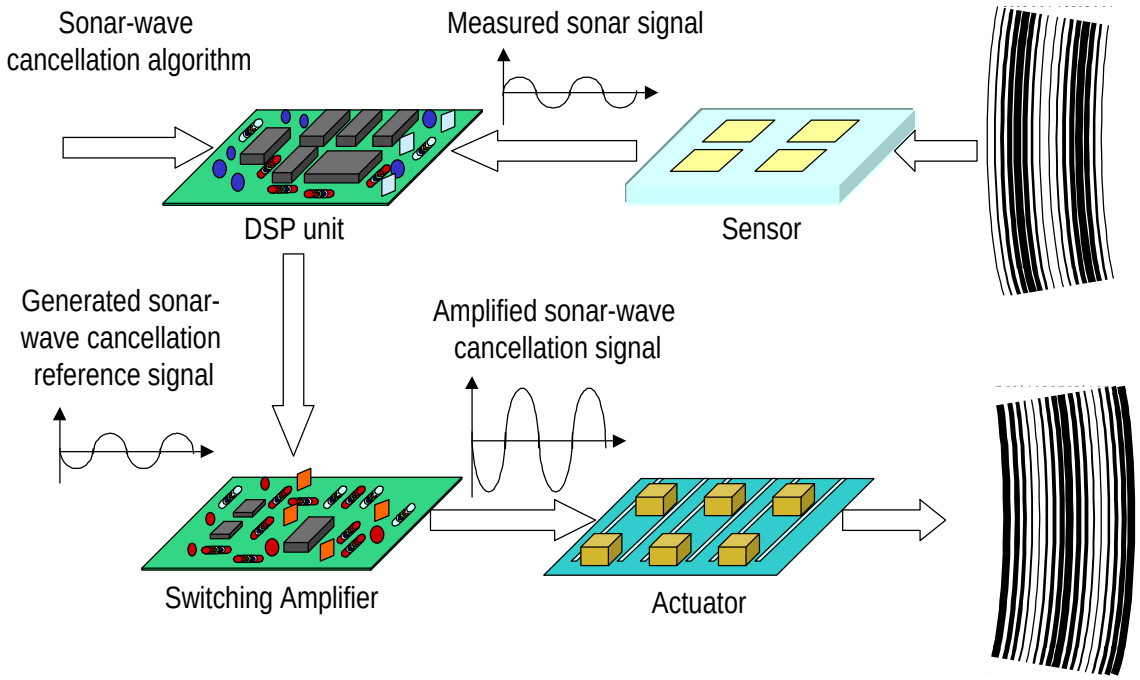

Figure 1.2 Block Diagram of Smart Materials Used for Sonar Wave Cancellation

1.2 Design Task and Technical Challenges

The design objective is to develop a power amplifier used to drive a smart material actuator array for underwater acoustic wave cancellation. The design specifications are:

- Power supply voltage: 32 volts
- Input signal frequency: 500 Hz~10kHz
- Output DC bias voltage: 14 volts
- Output AC voltage swing: ± 11 volts @ 500 Hz
- Output current capability: 1.6 A peak value
- Unit size: 3”x3”

The typical load for this switching amplifier is a smart material actuator array. Each actuator in this array is a stack electrostrictive material actuator as shown in Figure 1.3. The

electrostrictive actuator is made from PMN material, a smart material known for its high electrostrictive strain and relative low-hysteretic behavior.

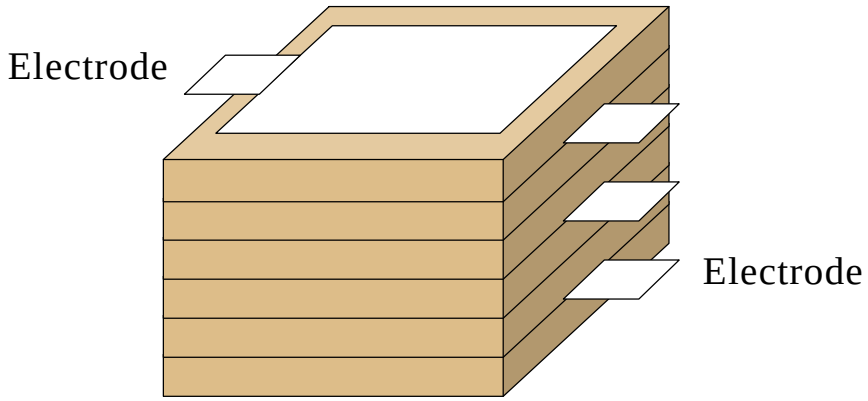

Figure 1.3 Sketch of an Electrostrictive Stack Actuator

The electrical characteristic of the actuator is highly capacitive. Figure 1.4 shows measurement results of the actuator's capacitance s.o. actuator's bias voltage. The x-axis is the DC voltage applied to the actuator, and the y-axis is the measured equivalent capacitance. The non-linear characteristic of the actuator is clearly shown in this figure. As the bias voltage increases from 0 to 22 volts, the capacitance varies from 32 μF to 5 μF in a nearly quadratic manner. In order to minimum the nonlinear effects of the actuator, a fixed 14 volts DC voltage is applied to the actuator as a bias voltage.

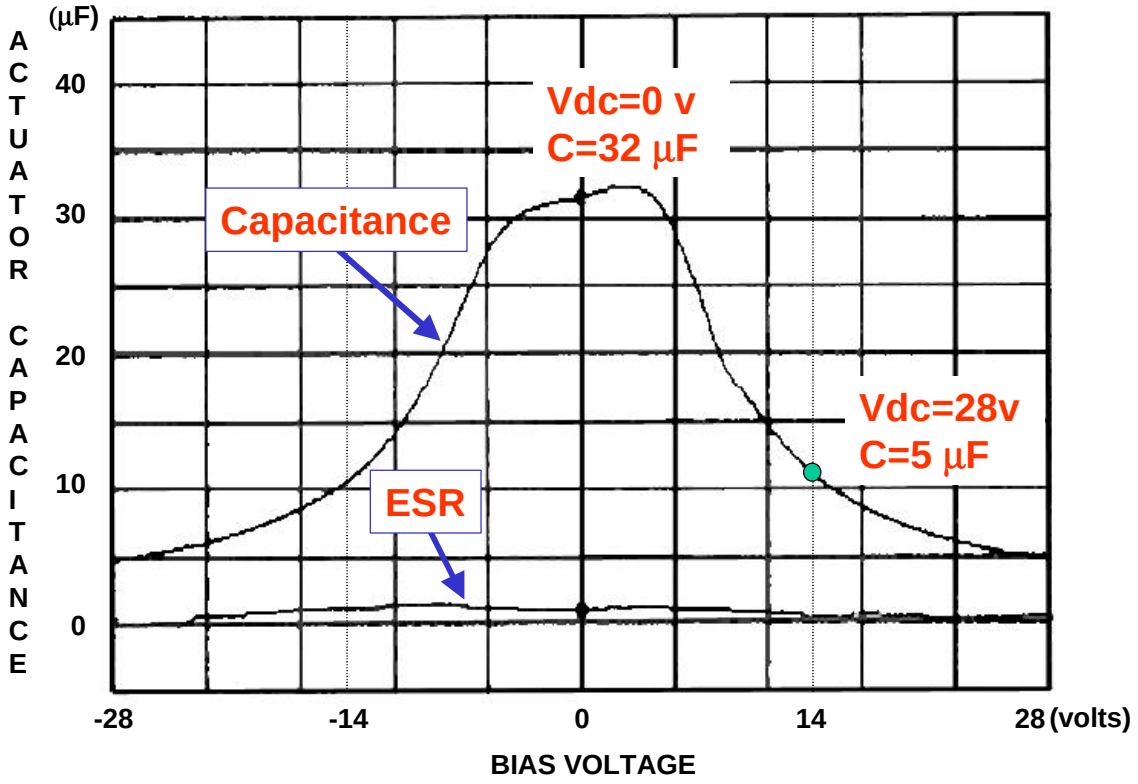

Figure 1.4 Electrostrictive Material Actuator Capacitance vs. Its DC Bias Voltage

Figure 1.5 shows the input and output signal relationship of the power amplifier. v_{ref} is the input reference signal to the amplifier, and v_{out}, i_{out} are the amplifier's output voltage signal and output current signal respectively.

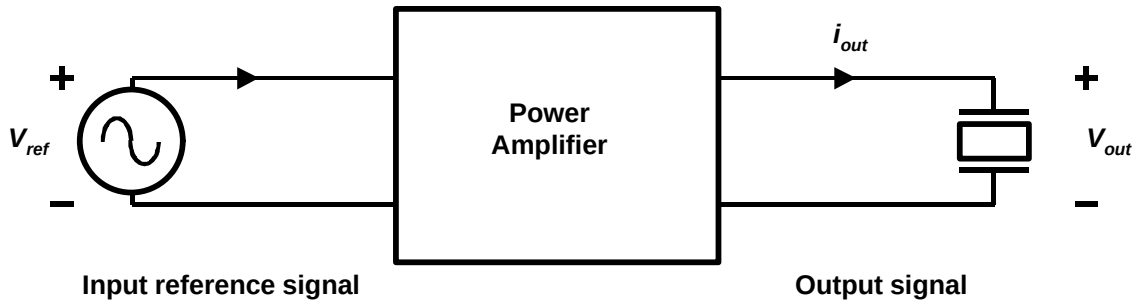

Figure 1.5 Input and Output Signal Relationship of the Power Amplifier

The desired amplifier's frequency response is shown in Figure 1.6. It requires that the amplitude of the output voltage signal to decrease at 20 dB per decade with respect to a constant-amplitude input reference signal ranging from 500 Hz to 10 kHz.

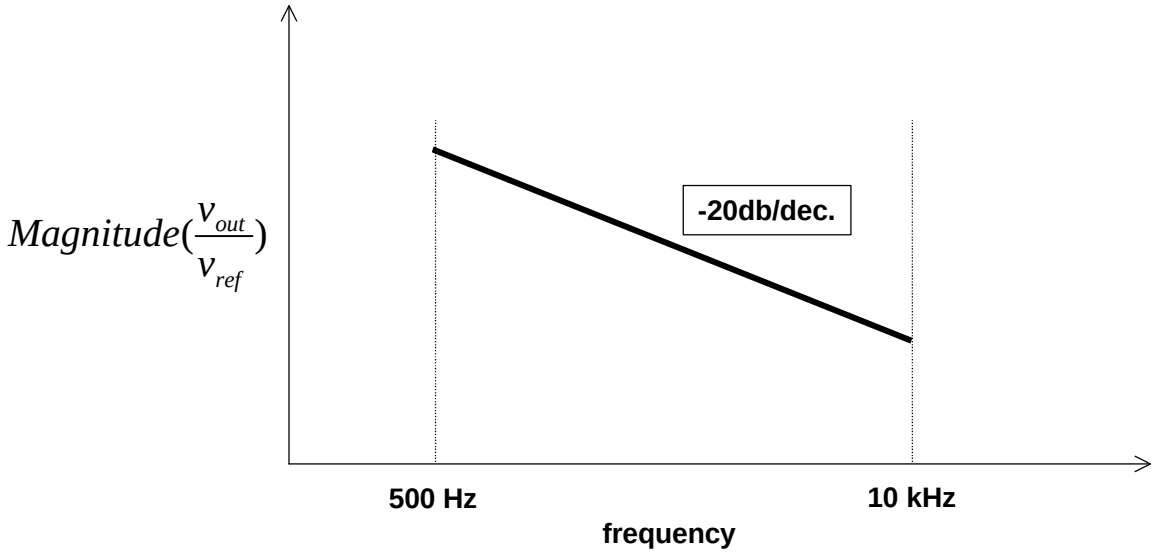

Figure 1.6 Frequency Response Requirement of the Power Amplifier

The purpose of this frequency response is to normalize the actuator velocity output with the reference signal input (Appendix 1)

1.3 Motivation of Research

Using electrostrictive materials for underwater acoustic wave cancellation is a new application for smart materials. This new application challenges the common practice of using linear power amplifiers as the driving devices for smart material actuators and demands a high efficiency, low profile switching amplifier design. This design work is motivated in the following aspects:

1. The demand for better power efficiency.

A simplified circuit schematic of a linear power amplifier is shown in Figure 1.7. This type of circuit is widely adopted as the power amplifier used to drive smart material actuators

[15-16]. Although it is simple and easy to get, the power efficiency of this power amplifier is usually very low.

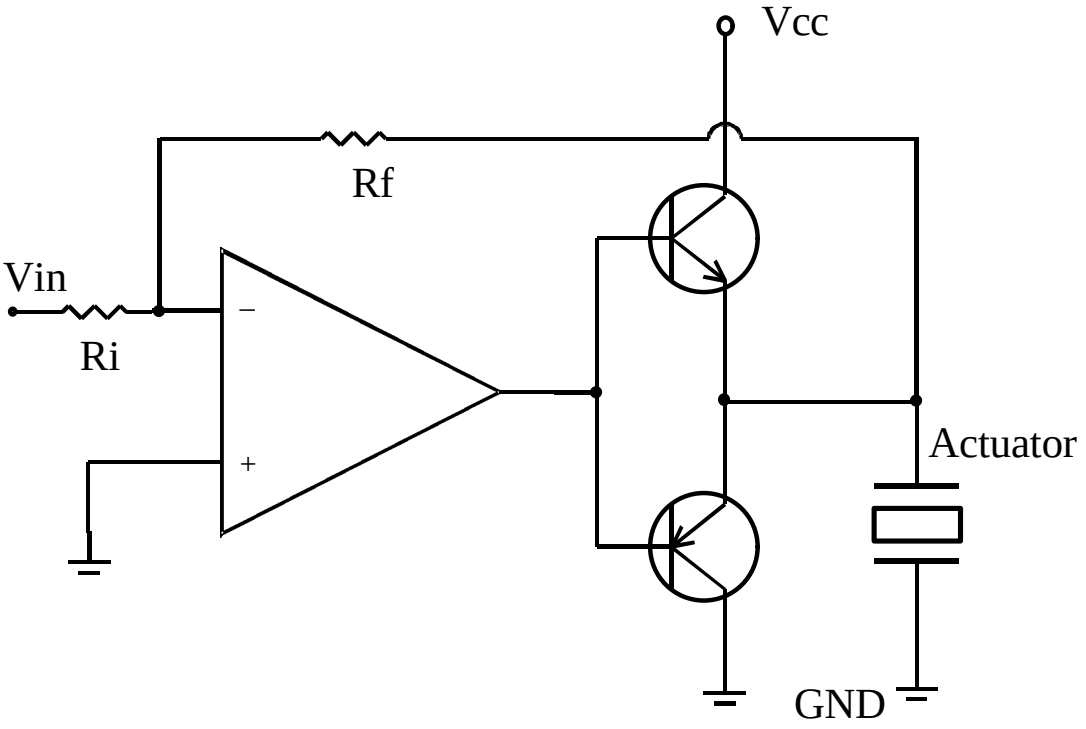

Figure 1.7 A Simplified Schematic of a Linear Power Amplifier

For example, a linear power amplifier is used to drive a piezoelectric actuator with a capacitance of C. In this case, the power dissipation of the amplifier can be estimated as [18]:

$$PD_{out,\max} = \frac{V_s^2}{2Z_L}\left|\frac{4}{p} - \cos q\right| \tag{1.2}$$

Where V_s is the amplifier supply voltage, Z_L is the magnitude of the load impedance, and q is the phase angle of the load impedance. q is 0° for resistive load, and 90° for pure reactive load.

It can be seen immediately that the power dissipation increases as the load property changes from resistive load to reactive load. This is due to the fact that linear power amplifiers can

not handle the bi-directional power flow. Instead of recycling the reactive power, the recycling energy is dissipated in the power amplifier's output impedance R_o in the form of heat. This poor power efficiency not only increases the total power drawn by the amplifier, but also increases the size of the amplifier because of the need of cumbersome heat sinks.

2. The possibility of using current mode control.

The most commonly used control law for the design of a linear power amplifier is output voltage control as shown in Figure 1.8.

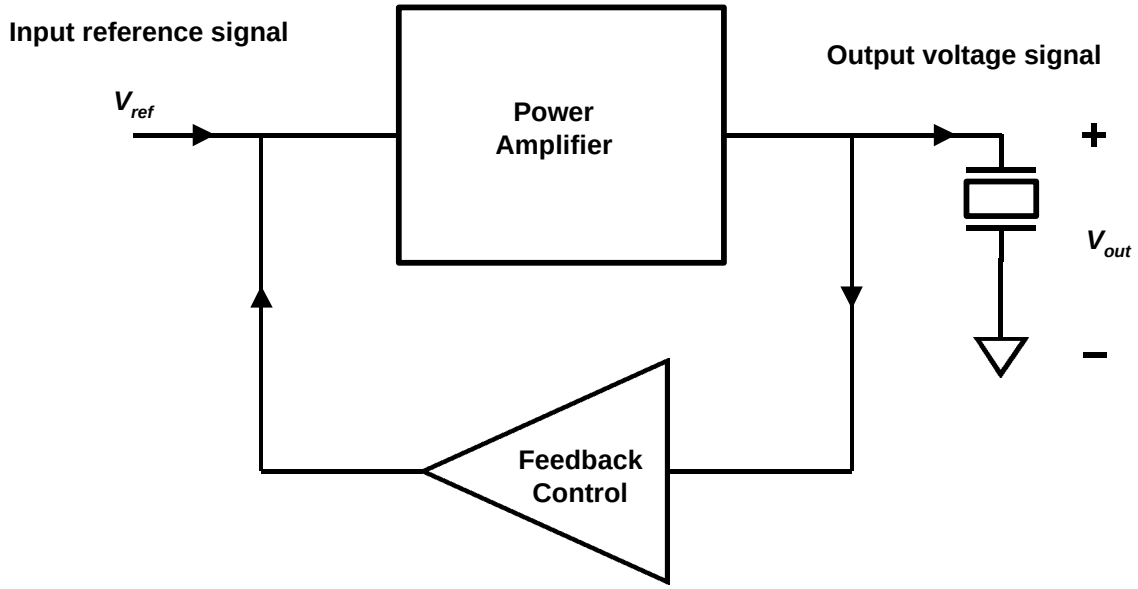

Figure 1.8 Block Diagram of Output Voltage Control Strategy

The principle of this voltage control strategy is based on the IEEE standard proposed by the committee of the IEEE Ultrasonics, Ferroelectrics and Frequency Control Society as the following equation [17]:

$$S = s^E T + dE \tag{1.3}$$

Where

S : strain,

s^E : elastic compliance at constant total field,

T : stress, and

d : piezoelectric constant.

If the thickness of the actuator is l, and the applied voltage is V, the electric field intensity E is readily available:

$$E = \frac{V}{l} \tag{1.4}$$

Substitute Equation (1.4) into Equation (1.3), and we get the piezoelectric constitutive relationships as the control law for output voltage control:

$$S = s^E T + d\frac{V_{out}}{l} \tag{1.5}$$

This control law predicts a linear relationship between the power amplifier's output voltage signal and the actuator's output displacement. It also assumes that the piezoelectric and electrostrictive actuators can be accurately driven open loop. This is not the actual case. Most of the piezoelectric and electrostrictive materials show various degrees of non-linearity and hysteresis [11] as is shown in Figure 1.9 and Figure 1.10.

Figure 1.9 shows one test result about the non-linear hysteretic characteristic of the piezoelectric material [5]. The x-axis is the electrical field intensity, and the y-axis is the micro-strain of the material. It can be seen that there is a nonlinear relationship between the electric field intensity and the actuator micro-strain. Furthermore, it can be seen that there is a prominent hysteretic loop when the piezoelectric materials are driven by electric field. This is due to the fact that most of the piezoelectric materials are ferroelectric materials and the ferroelectric effect manifests itself as hysteretic behavior [19].

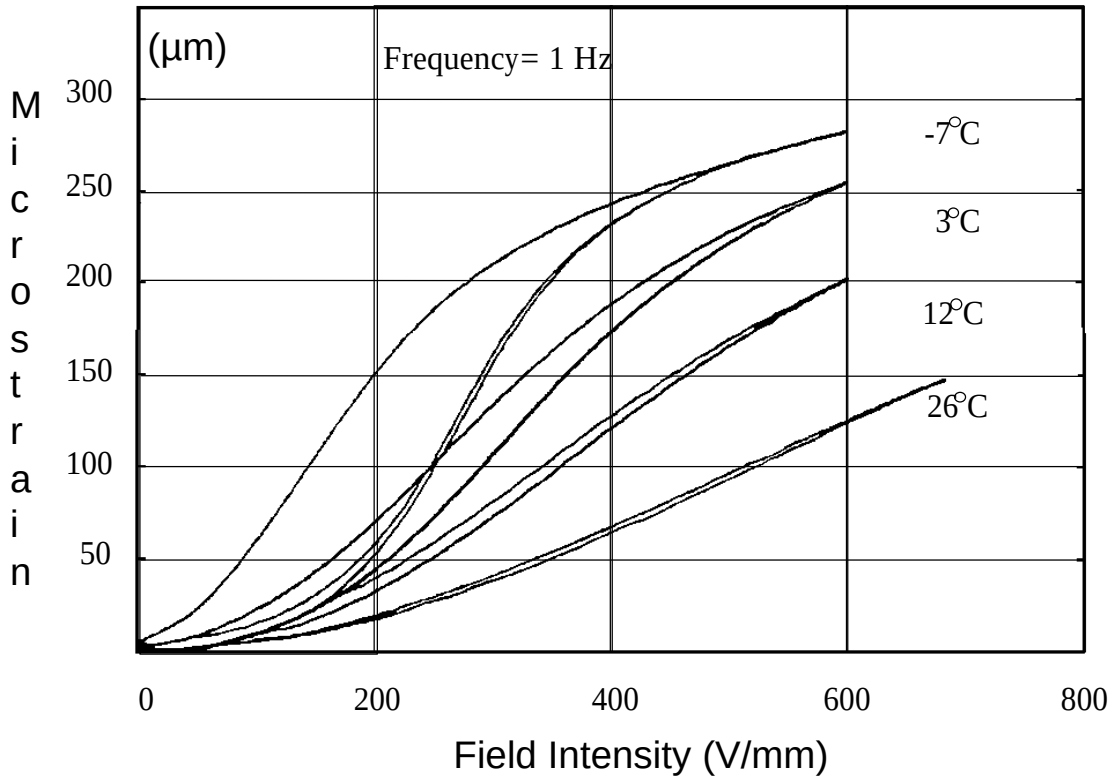

Figure 1.9 Non-linear Hysteretic Behaviour of Piezoelectric Materials

Figure 1.10 shows the relationship of the input AC signal with respect to the hysteretic curve of the actuator micro-strain. It can be seen that with each cycle of the AC signal excitation, the actuator's micro-strain travels in a hysteretic loop.

This hysteretic effect has severe impacts to the smart material applications. For example, in the acoustic wave cancellation application, this hysteretic behavior may reveal as a phase lag in the output acoustic wave, and reduce the effect of acoustic wave cancellation. In other applications like the precision position control, these hysteretic variations can cause position error as high as 20% of the total displacement output.

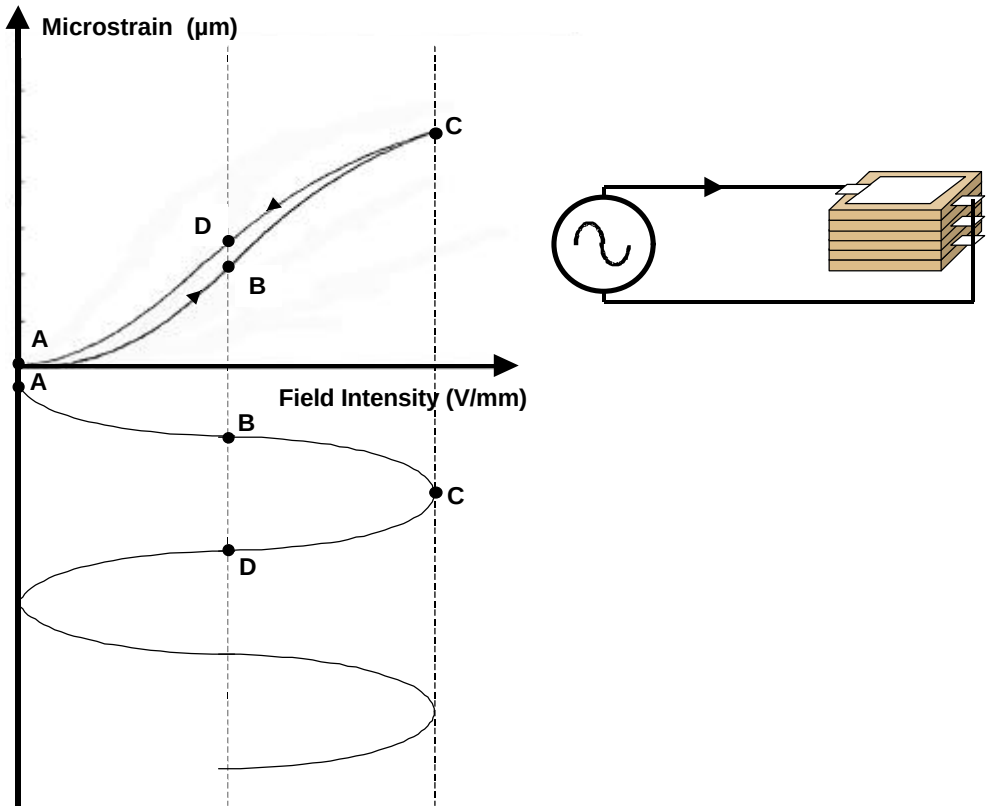

Figure 1.10 The Hysteretic Behavior of Piezoelectric Material

One way to alleviate this hysteretic problem is to use charge control instead of the commonly used voltage control. Recently studies have shown that the hysteretic behavior of the piezoelectric actuators can be greatly reduced if charge is used as the control variable instead of voltage [19-20]. Figure 1.11 shows the piezoelectric material displacement output when it is driven by voltage signal. The x-axis is the voltage input, and the y-axis is the piezoelectric material displacement output. The solid line shows the hysteretic behavior of the piezoelectric material when it is driven by AC voltage signal, and the dotted line is the tangential at the origin (which is predicted by Equation (1.5)). The difference between the voltage control law prediction and the actuator's actual displacement output is obvious.

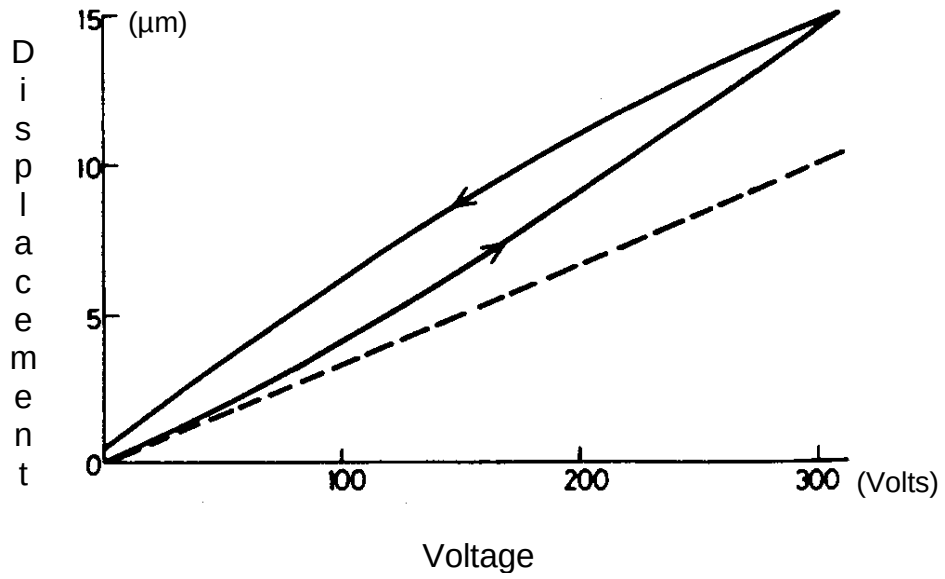

Figure 1.11 Piezoelectric Material Displacement Output Under Voltage Drive

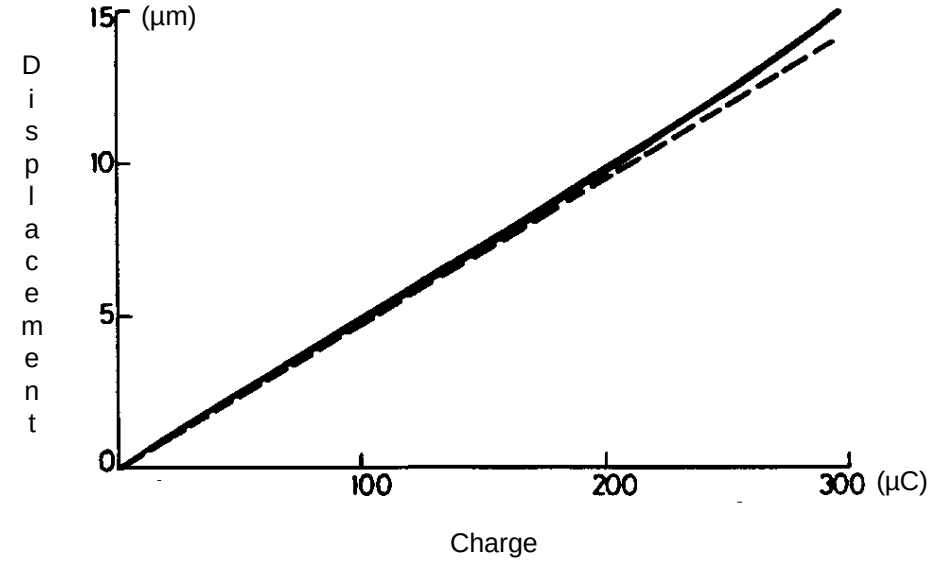

Figure 1.12 Piezoelectric Material Displacement Output Under Charge Drive

Figure 1.12 shows the piezoelectric actuator displacement output under charge drive. The solid line is the measured response of an actuator's displacement output. The dotted line is the tangential at the origin, and is predicted by the following curving fitting equation:

$$S = s^E T + d'Q \tag{1.6}$$

Where

d': coefficient of strain vs. charge

Q: applied charge

It can be seen that by using charge drive, the hysteresis and the non-linearity of the piezoelectric material are greatly reduced.

Other studies also validated that by using charge control instead of voltage control, the linearity of the piezoelectric materials can be improved and their hysteresis can be reduced [29-31].

In this switching amplifier design, we propose to use charge control law as the control method to reduce the non-linear hysteretic behavior of the actuator and to improve the control accuracy. The electric charge is estimated in two ways: by using peak current estimation and by using average current estimation.

An additional advantage of using this charge control law is that we can get directly control of the output velocity by simply control the output current. Take the derivative of Equation (1.6), we can get the following equation:

$$\frac{dS}{dt} = d'\frac{dQ}{dt} \tag{1.7}$$

$\frac{dS}{dt}$ is the actuator velocity, and $\frac{dQ}{dt}$ is nothing but the output current. Equation (1.7) indicates that the actuator velocity output can be directly manipulated by control the output current. If the circuit has a constant gain of output current to input reference signal, the velocity output of the actuator is automatically normalized.

1.4 Thesis Outline

This thesis includes 5 chapters, references and an appendix.

In Chapter 2, the power stage circuit design issues are discussed. When a power amplifier is designed to drive smart material actuators, it should be able to handle the circulating reactive power, otherwise the amplifier may run into significant thermal design and efficiency problems. A two-switch buck topology is used as the power stage in this switching amplifier design. The power stage design issues are discussed and the circuit operation principle is addressed. A small signal analysis of the power stage circuit is also done using the conventional model of the PWM switch to facilitate the future design work.

A switching amplifier design using peak current mode control is presented in Chapter 3. Theoretically, peak current mode control can approximate the charge delivered to the actuator during each switching cycle, and give better linearity since the actuator's displacement output has less hysteretic behavior when charge is used as the controlled variable rather than the output voltage. A switching amplifier prototype circuit using peak current mode control is developed with its small signal analysis. This prototype circuit is tested and its performance is evaluated.

Chapter 4 presents the switching amplifier design with average current mode control. The small signal analysis done in Chapter 2 reveals that the switching amplifier will have a low current loop gain at low frequencies when it is used to drive a capacitive load. However, due to the nonlinear nature of the smart material and the required signal bandwidth of the application, an evenly high current loop gain is very much desirable. An average current mode control strategy is proposed in this chapter to solve this problem. The design process is presented. A small signal analysis and a Pspice simulation are also given. The prototype circuit is tested and its performance is evaluated.

The design of the amplifier is concluded in Chapter 5. Current mode control can provide better linearity compared with the output voltage control due to the reduction of the material hysteretic behavior, and average current mode control will provide better current loop gain manipulation with regard to the peak current mode control. However, the non-

linear quadratic behavior of the electrostrictive materials is still not addressed and further work need to be done in the future.

CHAPTER 2. POWER STAGE DESIGN AND DEVELOPMENT

2.1 Introduction

The newly developed smart material application of underwater acoustic wave cancellation demands a high efficiency, low profile power amplifier design. Traditional linear power amplifiers do not have the capabilities to handle the circulating reactive power, therefore they tend to have an extremely low power efficiency in this application. This low power efficiency not only increases the total power the amplifiers drawn from their power supply, but also requires bulky heat sinks to dissipate the excessive heat. Thus the conventional linear power amplifier can not be used here.

One of the alternatives to a linear power amplifier design is a switching power amplifier [21-24]. For linear power amplifiers, most of the power consumption is caused by the linear operation of the power devices, in other words, the devices that handle the output current and voltage at the same time. For switching amplifiers, the power devices are working in either 'ON' or 'OFF' states. When the power devices are working in the 'ON' state, the voltages across the devices are low, so the devices' power consumption will be low. On the other hand, when the power devices are working in the 'OFF' state, there will be no current flow through the devices; thus the power consumption will also be low. By modulating the duration of the 'ON' and 'OFF' periods, the output of the switching amplifier (either voltage or current) can be controlled to follow the input reference signal, and thus the circuit can work as a power amplifier, and the expected efficiency will be higher than the linear power amplifiers.

In this thesis, the design issues of a switching power amplifier are addressed. Both peak current mode control and average current mode control have been tested to get the best

amplifier performance.

2.2 Power Stage Design

2.2.1 Topology and operation

Figure 2.1 shows the circuit block diagram for the switching power amplifier design. Buck topology is selected for the power stage circuit since the maximum output voltage will not exceed the input voltage range and there is no design requirement for isolation. Two bi-directional semiconductor devices are used to handle the bi-directional power flow generated by the reactive load, shown in Figure 2.1 as capacitor C. Since the semiconductor components are designed to work in either the 'ON' state or 'OFF' state, the power loss of this circuit will be essentially the turn-on and turn-off loss of the switches.

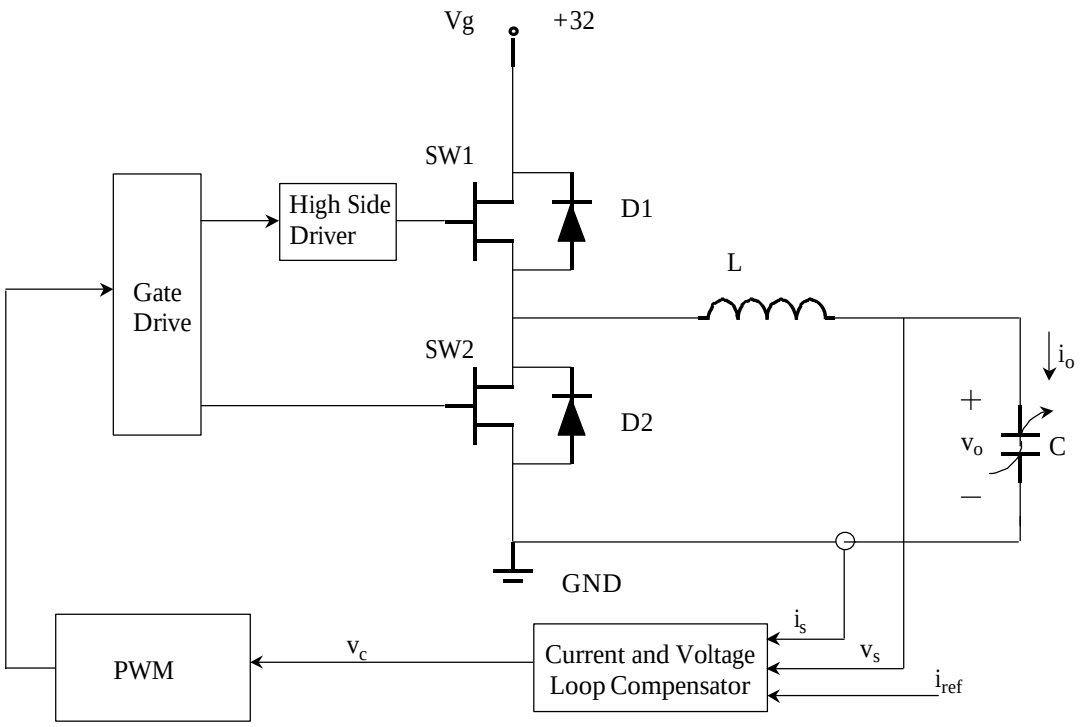

Figure 2.1 Block Diagram of a Switching Amplifier

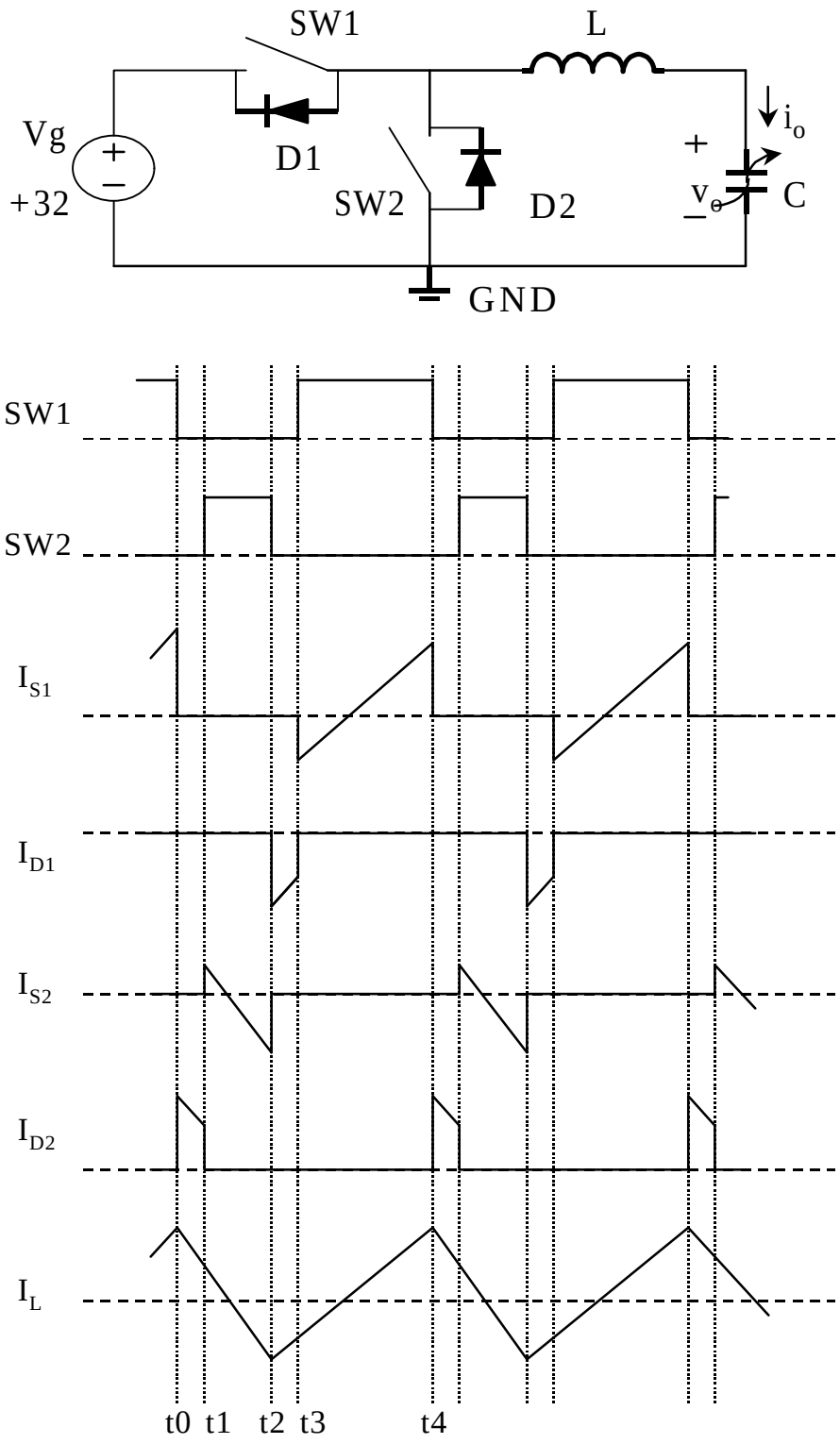

Figure 2.2 Operation of the Power Stage

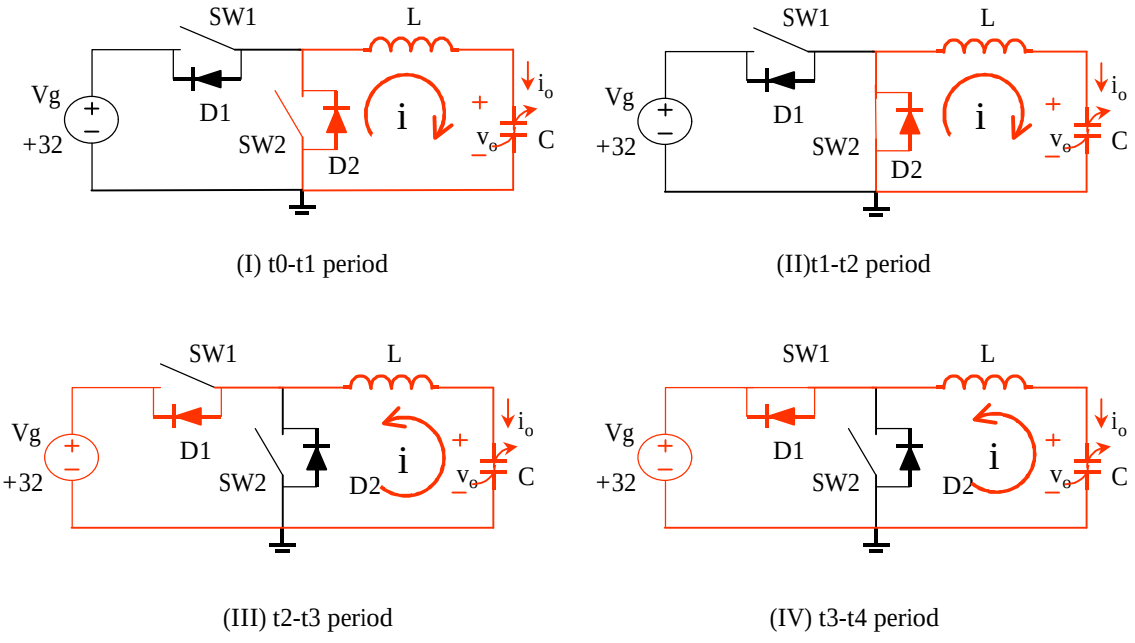

Figure 2.3 Four Power Stages of the Switching Amplifier

The power stage operation diagram of this switching amplifier is shown in Figure 2.2. Each cycle of the operation can be divided into four periods as shown in Figure 2.3.

(I) t0-t1 period

During time period t0 to t1, both SW1 and SW2 are off. The magnitude of the inductor current i_L begins to decrease, and this positive inductor current flows through D2. The voltage across switch SW2 is zero because of the conduction of D2. This period ends when SW2 turns on.

(II) t1-t2 period

In this time period, SW1 is turned off. D1 is also off due to reverse bias voltage. SW2 turns

on, and current flows through SW2. Since diode D2 is conducting while SW2 is turned on, SW2 is working at zero voltage switching mode. The magnitude of the inductor current keeps decreasing and at the end of this period, the direction of the inductor current reverses as the result of the resonance of the inductor L and load capacitance C. This period ends when SW2 is turned off.

(III) t2-t3 period

During the time period t2 and t3, both SW1 and SW2 are turned off. Since the inductor current is negative, D2 is also turned off. The flux in the inductor L forces the current to flow through D1 to charge the input power supply. The magnitude of the inductor current is decreasing. This period ends when SW1 is turned on.

(IV) t3-t4 period

During this time period, SW1 turns on, SW2 is off, diode D2 is also turned off by the input voltage V_g, and current flows through SW1. Since SW1 is turned on at the time when D1 is on, SW1 is also working at ZVS mode. The magnitude of the inductor current begins to increase during this time period, and continues to increase until it ends when SW1 is turned off.

2.2.2 Power stage design

Power stage design issues includes the selecting switching frequency and switching components; designing of the duty cycle; designing of the inductor; and other related design problems.

2.2.2.1 Switching frequency

The switching frequency for the switching amplifier design is selected as a trade-off between the amplifier's current loop crossover frequency and the amplifier's power stage efficiency. Since the main switches of the switching amplifier work in either 'on' or 'off' states, most of the power stage power losses come from the switches' turn-on and turn-off loss. If the

power stage has a turn-on loss of $Loss_{on}$ and a turn-off loss of $Loss_{off}$, and the switching frequency is f_{sw}, the total loss $Loss_{total}$ is given by:

$$Loss_{total} = (Loss_{on} + Loss_{off}) f_{sw} \tag{2.1}$$

Equation (2.1) shows that total power loss is directly proportional to the switching frequency.

On the other hand, for a buck converter with current-injection control, the current loop gain is approximated by [26]:

$$T_i(s) \cong \frac{L}{RT_s m_c D'} \frac{1+sCR}{\Delta(s)} H_e(s) \tag{2.2}$$

Where

$$\Delta(s) = 1 + \frac{s}{w_0 Q_{ps}} + \frac{s^2}{w_0^2} \tag{2.3}$$

$$Q_{ps} = \frac{1}{w_0 [\frac{L}{R} + CR_c]} \tag{2.4}$$

$$w_0 = \frac{1}{\sqrt{LC}} \tag{2.5}$$

$$H_e(s) \cong 1 + \frac{s}{w_n Q_z} + \frac{s^2}{w_n^2} \tag{2.6}$$

Equation (2.2) shows that increasing switching frequency will increase the current loop gain, and thus increase the current loop crossover frequency once the current loop feedback is given.

In this switching amplifier design, the input signal bandwidth is between 500 Hz and 10 kHz. The current loop should have a minimum loop-gain crossover frequency well above 60 kHz. Different switching frequencies have been chosen and their experimental results are compared, and a switching frequency of 280 kHz was chosen as a reasonable compromise between the current loop crossover frequency and the MOSFET switching loss.

2.2.2.2 Duty cycle range

The variation of the duty cycle is very large in this amplifier design since the output voltage varies from the minimum output voltage, three volts, to the maximum output voltage, 25 volts. The duty cycle is 0.44 when there is no AC signal input, and the output voltage is the 14 volts DC bias voltage. With AC signal input, the maximum duty cycle range is from 0.09 to 0.78.

2.2.2.3 Selection of switch components

The selection of the switching components is based on the switching frequency and power level in the circuit design. Since this circuit uses a switching frequency of 280 kHz and the power rating is in the range of 100 watts, MOSFETs are chosen as the main switches in the power stage design.

As can be seen from Figure 2.3, the power flow in the output stage is bi-directional. At a certain time, there is current flowing through the power switch to charge the capacitive load while at other times, this current flows back from the load and charges the power supply.

This bi-directional power flow increases the circuit's supply efficiency, but it also requires bi-directional power switches to be able to handle the bi-directional current properly.

A MOSFET and its body diode can constitute a bi-directional power switch. This switch configuration is simple and saves both design cost and component space. However, since the body diode of a MOSFET is usually slow, it may cause a severe reverse recovery problem. In this power stage design, two methods are used to avoid the diode's reverse recovery problem:

1. Use ZVT scheme in the power stage design. As shown in Section 2.3.1, both the diodes D1 and D2 are turned off by the turn on of the MOSFETs. This ZVT operation provides soft turn-off of the diodes, although it cannot completely eliminate the reverse recovery problem.

2. Use an ultra-fast HDTMOS E-FET power field effect transistor which has a very fast reverse recovery body diode. Motorola MTD20N06 MOSFET is used because of its excellent turn-on resistance and ultra-fast body diode [27]. The body diode of this MOSFET has a diode reverse recovery time $t_{rr} = 35.7$ nS, which is comparable with some of the best Schottky diodes. The drain to source resistance $R_{DS(on)} = 0.035\,\Omega$, which gives it a very low 'ON' resistance.

2.2.2.4 Inductor design

The maximum inductor current can be estimated from the load capacitance as follows:

$$\mathrm{I}_{max} = C_{load} \cdot \frac{dv}{dt} \tag{2.7}$$

The calculated inductor peak current is approximately 1.6 A. Because of the circuit volume

constraint, the size of the inductor is limited. Considering that smart material actuators are relatively insensitive to the high frequency ripple current, the output inductor is designed to have a 25% output current as its ripple current to reduce its physical size. The maximum ripple current will be 3.2*25%=0.8 A.

This design results in an inductor value of 30 μH. As the inductor works at 280 kHz, a high frequency iron power core Micrometals T80-52 is used [28] with 26 turns of AWG18 wire, and the actual inductance is measured as 30 μH.

2.3 Power Stage Small Signal Modeling

In switching amplifier design, the power stage circuit handles the output current and voltage, while the control loop plays an important role in the optimizing of the overall amplifier performance.

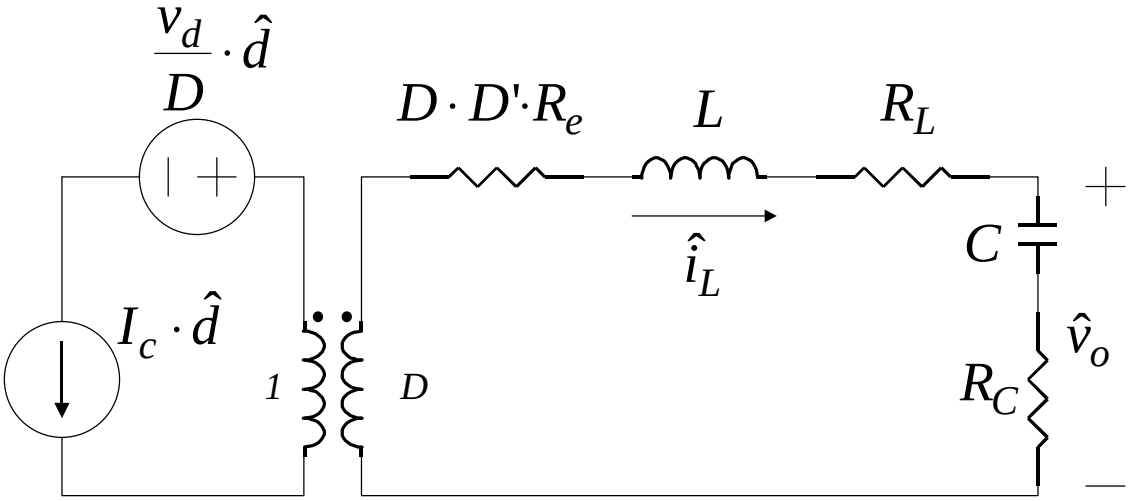

Figure 2.4 Power Stage Small Signal Model

In order to design and optimize the control loop, a power stage small signal model is developed using the PWM switch model as shown in Figure 2.4, where L is the output inductance, and C is the load capacitance [25]. This small signal model will be used in the

following chapters as it is given here.

The duty cycle to output voltage transfer function is given by [26]:

$$\frac{\hat{v}_o(s)}{\hat{d}(s)} = \frac{Vg}{L \cdot C} \cdot \frac{sCRc + 1}{s^2 + s \cdot [\frac{Rc}{L} + \frac{1}{RC}] + \frac{1}{LC}} \tag{2.8}$$

The control voltage to output inductor current transfer function is given by [26] Equation (2.9):

$$\frac{\hat{i}_L(s)}{\hat{d}(s)} = \frac{Vg}{L} \cdot \frac{s}{s^2 + s \cdot [\frac{Rc}{L} + \frac{1}{RC}] + \frac{1}{LC}} \tag{2.9}$$

Where

V_g : Input voltage

L : Output inductor

C : Output Capacitor (actuator capacitance)

R_c : Capacitor ESR

R : Load resistance

d : Duty cycle

i_L : Inductor current

v_o : Output voltage

The duty cycle to output voltage transfer function is shown in Figure 2.5, and duty cycle to

inductor current transfer function is shown in Figure 2.6. From Figure 2.5, we can see that the duty cycle to output voltage transfer function is pretty flat within the 500 Hz to 10 kHz range. However, from the duty cycle to inductor current transfer function, we can see the influence of a reactive load. Unlike a buck circuit with a typical resistive load, the duty cycle to output current transfer function of this circuit will not have a low frequency zero which is originated from the output capacitor and the load resistor. The low frequency current loop gain will increase with a 20 dB/dec slope from very low frequency (resonant frequency of the inductor ESR and the load capacitor) to the output LC resonant frequency where the double pole is. The direct impact of this transfer function is a low frequency current loop gain. These zeroes are formulated by the load resistor with the output capacitor and output inductor respectively. If there is a low frequency zero Z1 generated by the load resistor and output capacitor, the output stage current loop gain will be flat before the frequency of Z1 and therefore the low frequency current loop gain will be approximately the loop gain value at the frequency of Z1. If there is no load resistor to form such a zero, the low frequency current loop gain will start from a much smaller value and maintain its increasing slope until it reaches the frequency of the power stage double pole. So the low frequency current loop gain will be smaller.

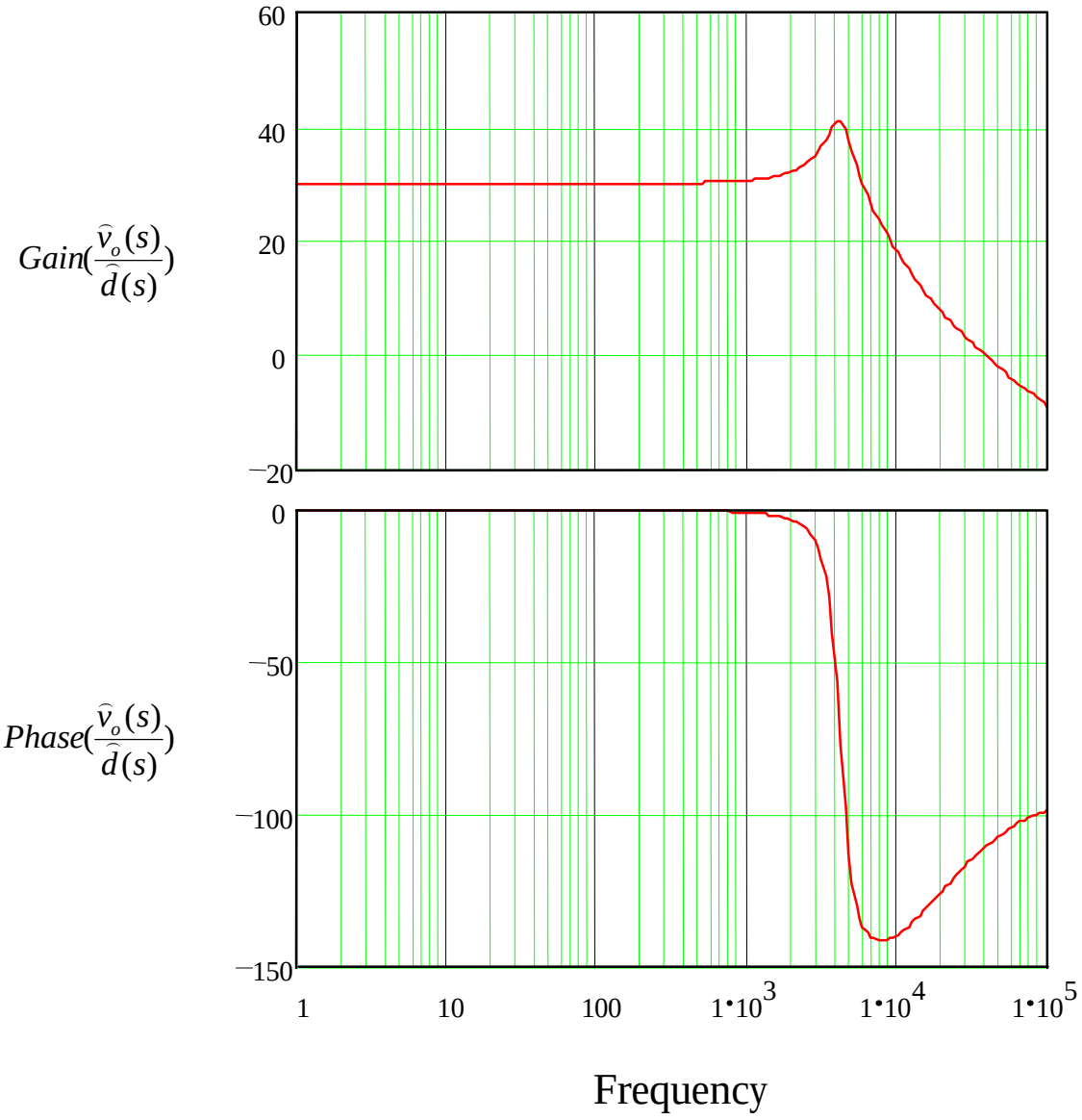

Figure 2.5 Bode Plot of Duty Cycle vs. Output Voltage

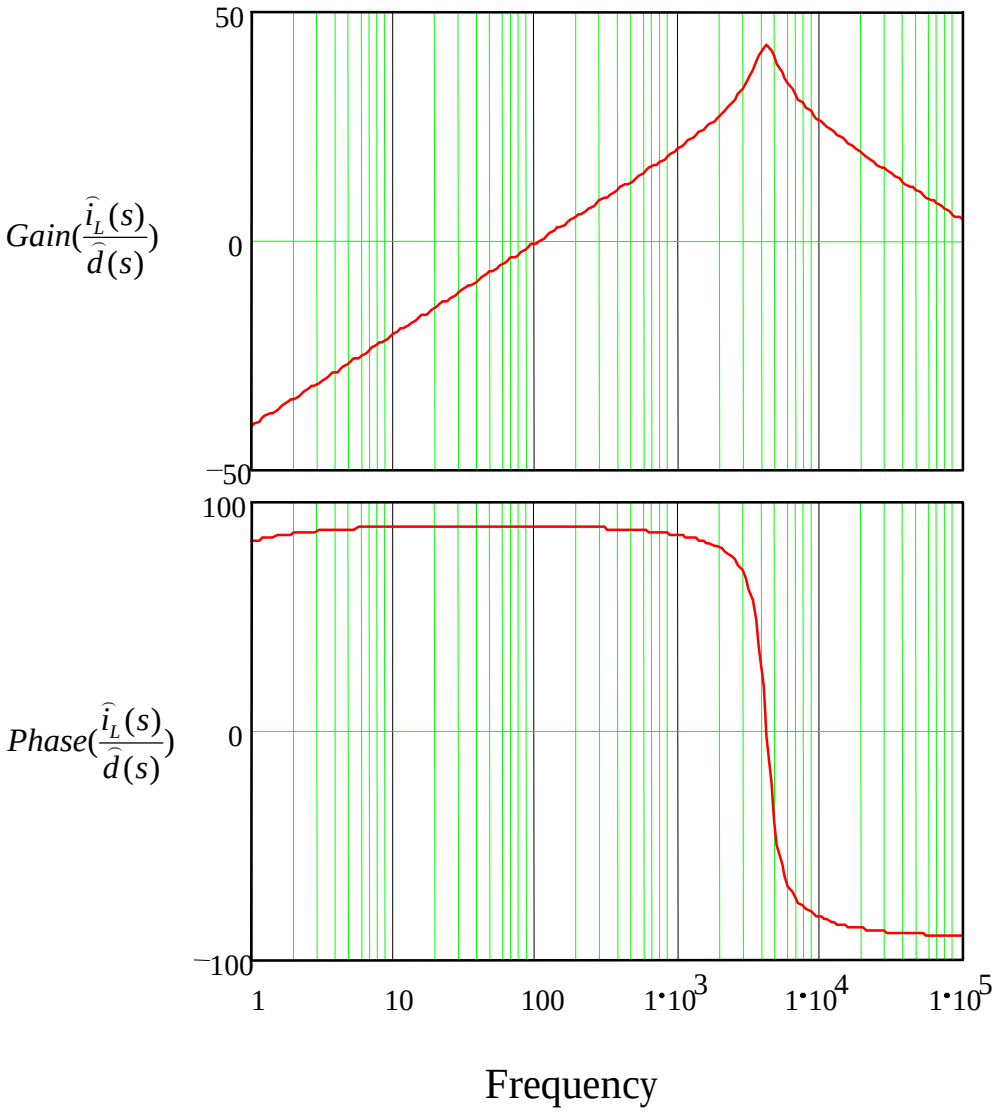

Figure 2.6 Bode Plot of Duty Cycle vs. Output Current

2.4 Power Stage Experimental Results

The open-loop power stage efficiency is tested to evaluate the performance of the circuit.

Using a resistive load, the power stage efficiency is tested for different output. The circuit is tested under the following conditions:

Input voltage: 28 volts

Output voltage: 14 volts

MOSFETs: MTD20N06

Switching Frequency: 280 kHz

PWM controller: UC3823

Load: Resistor

The test result is listed in Table 2.1 and plotted in Figure 2.7.

Table 2.1 Efficiency vs. Output Power

R	Input Current (A)	Output Current (A)	Input Power (W)	Output Power (W)	Efficiency
46	0.15	0.29	4.2	4.07	96.94%
23	0.31	0.58	8.68	8.13	93.65%
15	0.47	0.89	13.16	12.45	94.65%
12	0.58	1.11	16.23	15.53	95.66%
10	0.7	1.33	19.59	18.65	95.17%
9	0.77	1.48	21.55	20.72	96.14%
8	0.86	1.66	24.08	23.24	96.51%
7	0.98	1.88	27.44	26.32	95.92%
6	1.13	2.16	31.63	30.22	95.54%

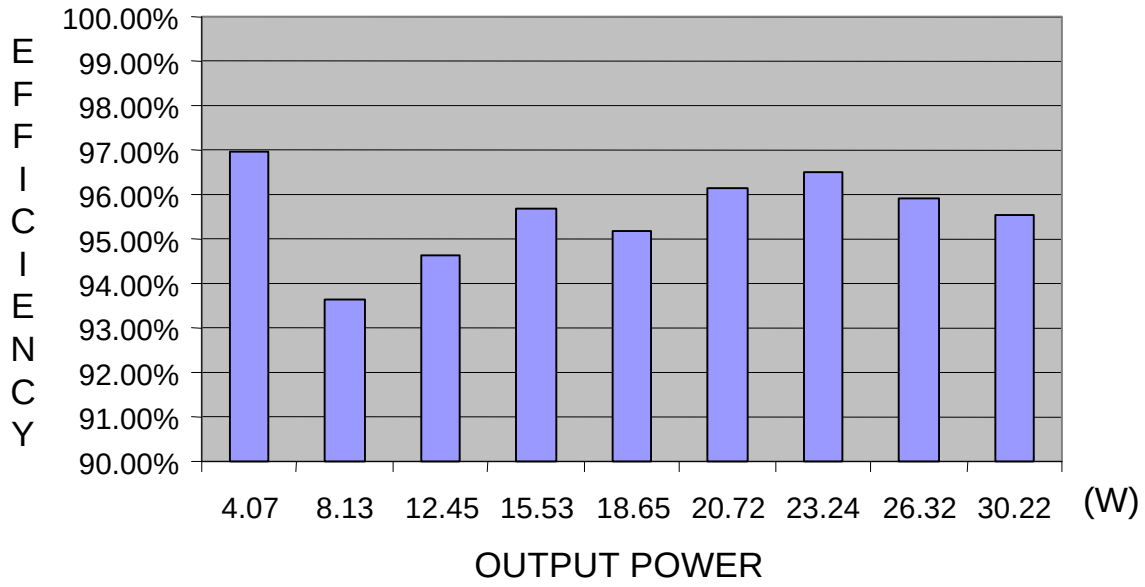

Figure 2.7 Power Stage Efficiency vs. Output Power

It can be seen that the power stage efficiency is around 90% with constant DC voltage output.

CHAPTER 3. PEAK CURRENT MODE CONTROL CIRCUIT DESIGN

3.1 Introduction

The widely accepted control law for piezoelectric and electrostrictive material actuators is output voltage control as rewritten in Equation (3.1).

$$S = s^E T + d\frac{V_{out}}{l} \tag{3.1}$$

Although easy to apply, the actuators will show heavy hysteretic behavior when they are driven by external voltage signal (as shown in Figure 1.9, Figure 1.10 and Figure 1.11) and thus this hysteretic behavior will greatly affect the actuators' displacement output accuracy.

The alternative for output voltage control is charge control, as rewritten in Equation (3.2),

$$S = s^E T + d'Q \tag{3.2}$$

As can be seen from Figure 1.12, the actuator's hysteretic behavior will be greatly reduced if charge control method is used.

Since

$$Q = \int_t^{t+T} i(t)dt \tag{3.3}$$

Equation (3.2) can be rewritten as:

$$S = s^E T + d' \int_t^{t+T} i(t)dt \tag{3.4}$$

Take the derivative of Equation (3.4), we can get:

$$\frac{dS}{dt} = d' \cdot i(t) \tag{3.5}$$

The left hand side of Equation (3.5) is the actuator velocity that we want to control, and the right hand side is the average output current flowing into the actuator (due to the limitation from its mechanical structure, the actuator cannot respond to the frequency as high as the switching frequency). As shown in Figure 3.1, if the output peak current is used as the control variable, then we get the peak current mode control as following:

$$\frac{dS}{dt} = d' \cdot i_{pk}(t) \tag{3.6}$$

As shown in Figure 3.1, the peak of the inductor current is following the input reference signal when peak current mode control is used in the circuit design, while the average output current is approximately following the input reference.

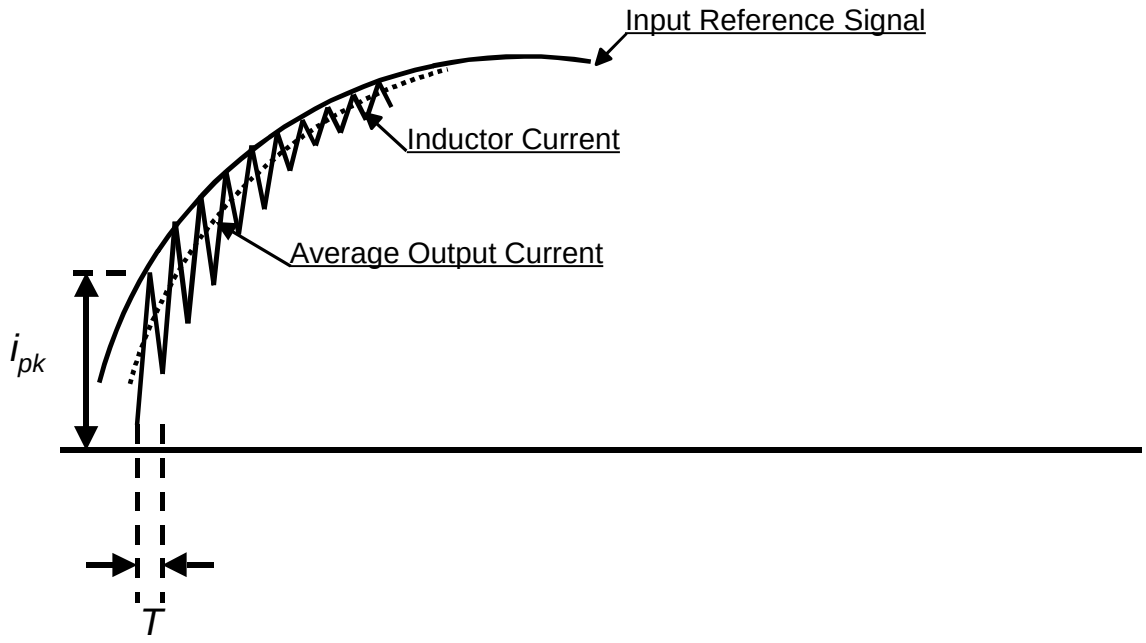

Figure 3.1 Principal of Peak Current Mode Control

Equation (3.6) indicates that the peak charging current of the smart material actuator can be used as a control variable in the design of a control circuit for the switching amplifier.

3.2 Small Signal Modeling of Peak Current Mode Control

3.2.1 Current loop design

The current loop compensator for a peak current mode control circuitry is a pure gain stage. This gain is determined by the gain of the current sensor and the gain of current loop amplifier. The current loop compensator transfer function is given by:

$$G_c(s) = w_i \tag{3.7}$$

In order to avoid the sub-harmonic oscillation, an external ramp is used to ensure the current loop will remain stable for duty cycles larger than 50%.

The current loop gain is given by:

$$T_i(s) = F_m H_e(s) G_c(s) \frac{\hat{i}_L(s)}{\hat{d}(s)} \tag{3.8}$$

Where $H_e(s)$ is the sampling gain shown in Equation (2.6).

The current loop gain of peak current mode control is shown in Figure 3.2.

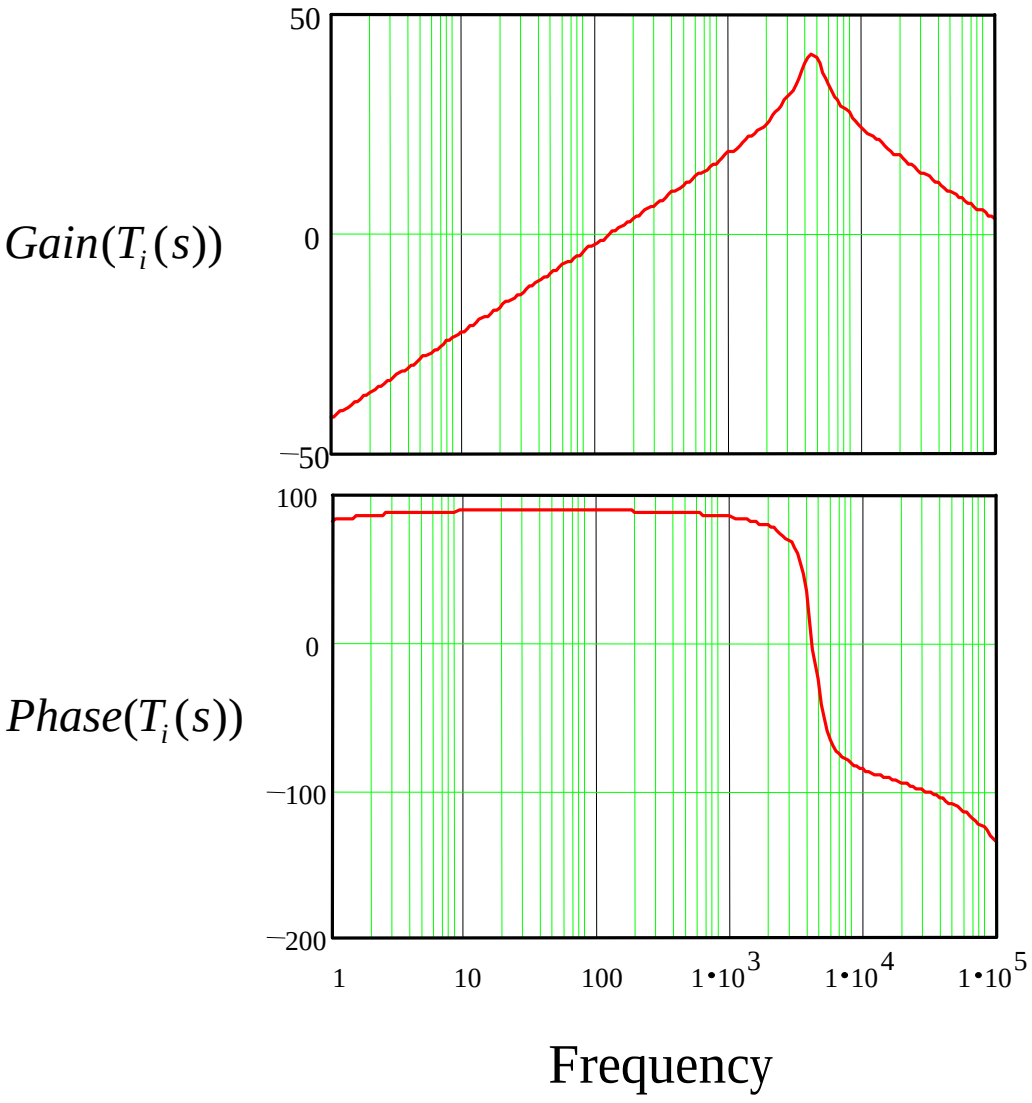

Figure 3.2 Current Loop gain Using Peak Current Mode Control

3.2.2 Voltage loop design

The voltage control loop regulates the switching amplifier's DC output voltage and this DC output voltage is used as the bias voltage for the PMN actuator. Because of the non-linear behavior of the PMN material, the voltage across the actuator $v(t)$ and the current charging the actuator $i(t)$ has the following relationship:

$$i(t) = C[v(t)]\frac{dv(t)}{dt} \tag{3.9}$$

Where $C[v(t)]$ is the instantaneous actuator capacitance at actuator voltage $v(t)$, as shown in Figure 1.4, and $C[v(t)]$ is a non-linear function of $v(t)$.

The non-linear behavior of $C[v(t)]$ suggests that there is a complex relationship between the actuator charging current and the actuator output voltage. Since only the charging current is the desired control variable, the current control loop and the voltage control loop are designed to be separate from each other. The current control loop will have a bandwidth cover the whole working frequency and the voltage control loop will have a very low crossover frequency that is at least one decade lower than the required signal bandwidth. Since the input signal bandwidth is 500 Hz to 10 kHz, the crossover of the voltage control loop is chosen to be 50 Hz.

The voltage loop compensator transfer function is given by:

$$G_v(s) = w_v \frac{1+\frac{s}{w_z}}{s} \tag{3.10}$$

w_z is a zero which is placed at approximately one decade below 500 Hz. This zero will help to cancel the effect of the origin pole after the crossover frequency, so it will help to give a flat frequency response in the voltage control loop within the 500 Hz to 10 kHz input frequency range.

3.3 Peak Current Mode Control Design and Experiment Results

A prototype circuit using peak current mode control is built using UC1823 as the PWM controller. The circuit's closed-loop PSPICE simulation is shown in Figure 3.3. It can be seen that the outer loop gain T2 has a crossover frequency at 15.2 kHz. Figure 3.4 shows the closed-loop output current to input reference signal transfer function. The magnitude variation within the 500 Hz to 10 kHz bandwidth is about 2.5 dB, and the phase variation is about 27°. It can be further noticed that the phase lead at 500 Hz is about 20°, which is very large in the application of sonar wave cancellation.

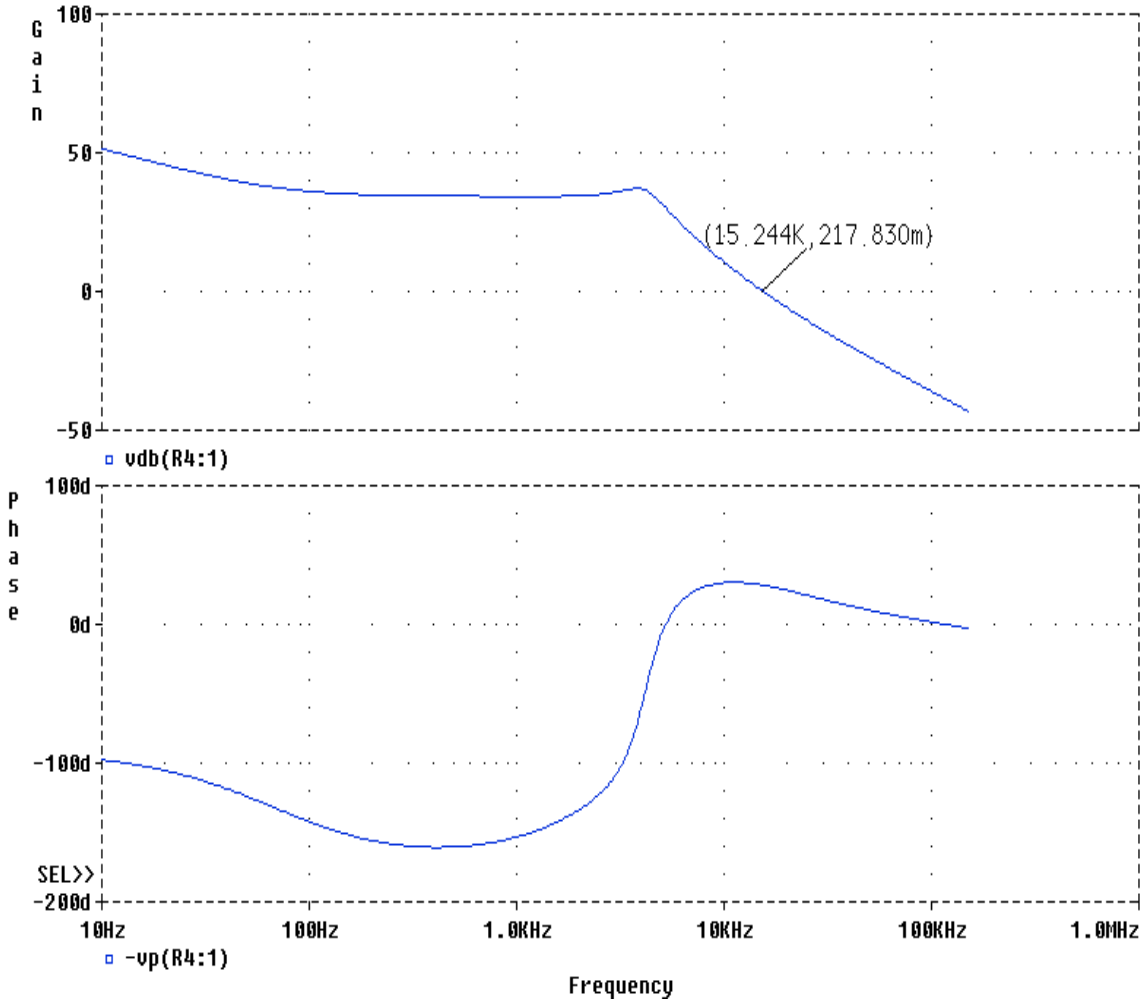

Figure 3.3 Outer Loop Gain Simulated by Pspice Small Signal Model

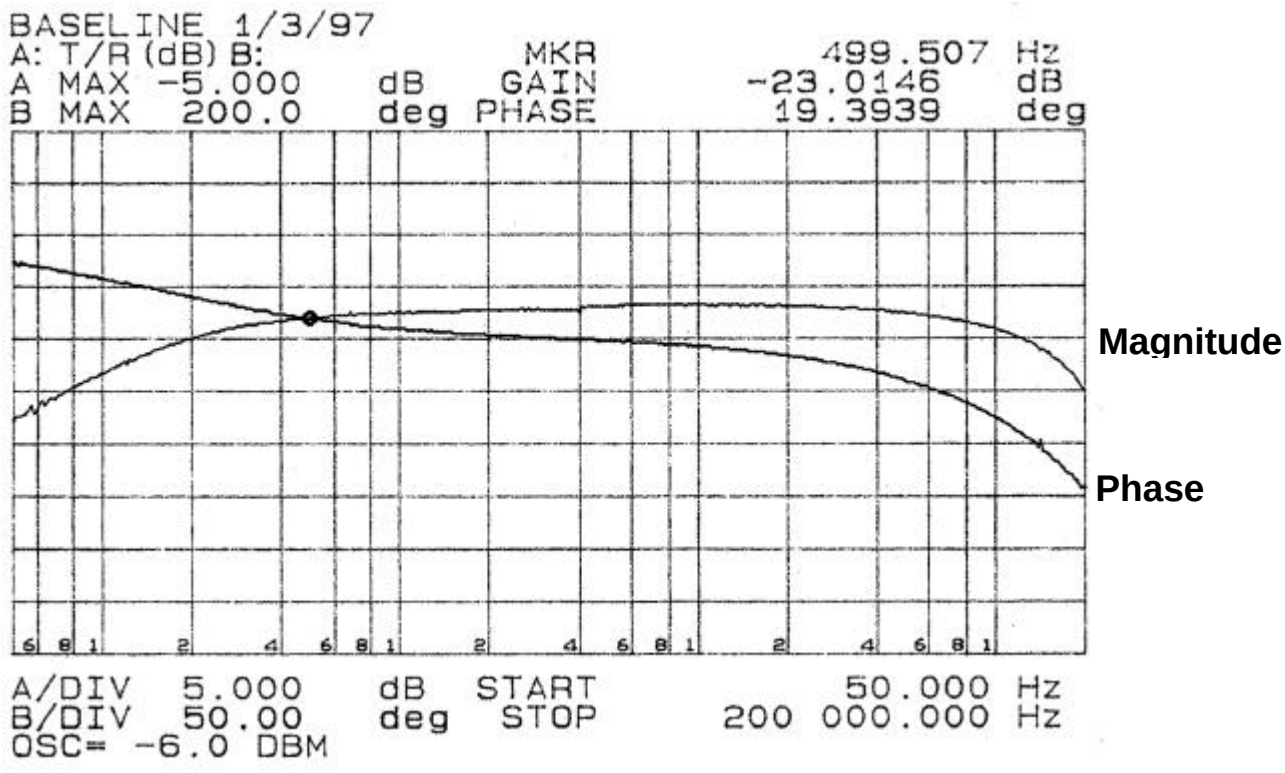

Figure 3.4 Closed-loop Output Current to Input Reference Signal Transfer Function

Figure 3.5 and Figure 3.6 show the prototype switching amplifier circuit using peak current mode control. Figure 3.5 shows the control circuit which is to the left side of the picture, and the power stage circuit which is to the right of the picture. Figure 3.6 is the upper view of the switching amplifier, shows the smart material actuator array when it is mounted on top of the prototype circuit.

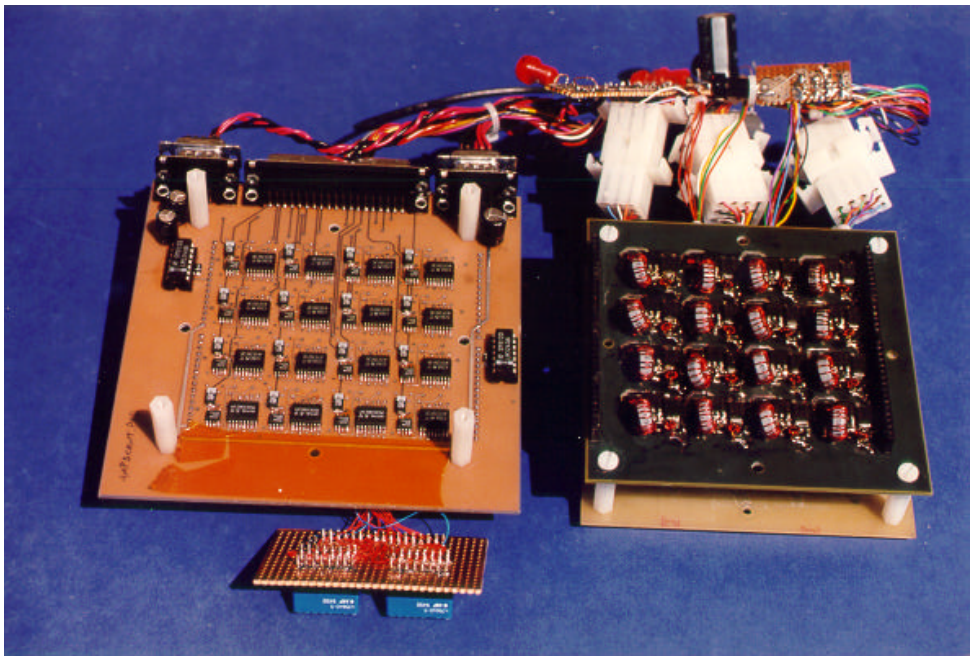

Figure 3.5 View of a Prototype Switching Amplifier Using Peak Current Mode Control

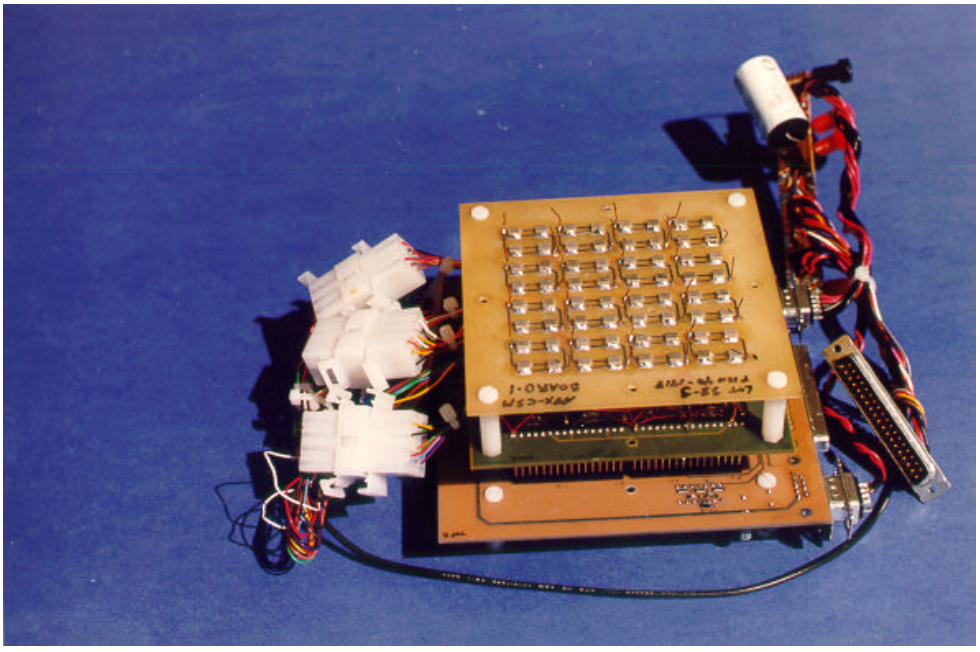

Figure 3.6 View of a Prototype Switching Amplifier with Smart Material Actuators Mounted on Top of the Amplifier

Figure 3.7 and Figure 3.8 show the output current waveform. The upper most trace is the voltage output waveform, the middle waveform is the output current, and the bottom one shows the input current reference signal. Figure 3.7 is the current waveform taken at input signal frequency=500 Hz, and Figure 3.8 is taken at 10 kHz. They both show that the output current follows the input current reference signal. It should also be noted that there is 90° phase shift between the output voltage signal and input current reference signal; this shows the results of current mode control.

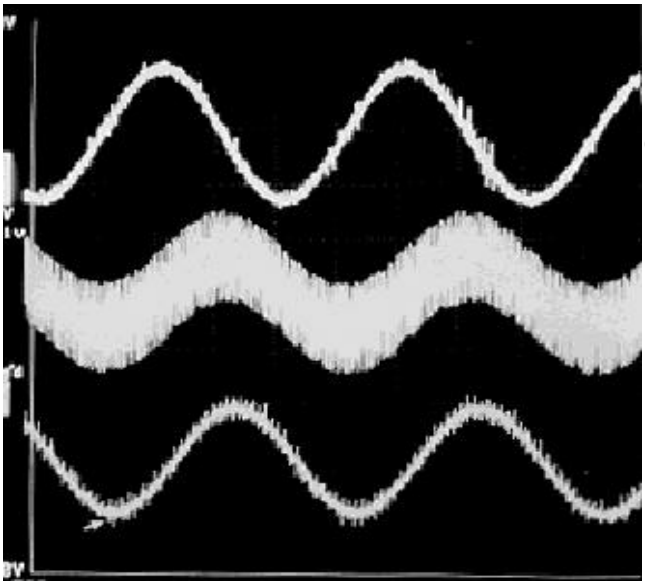

Figure 3.7 Output Voltage and Current Waveform at 500 Hz

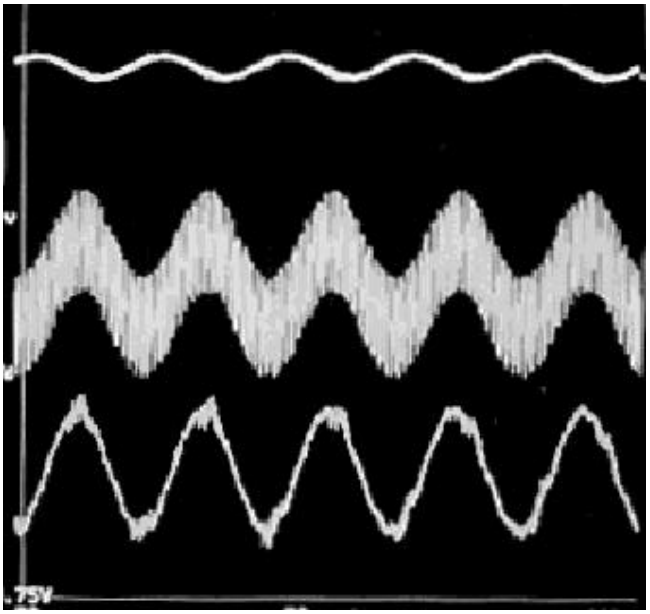

Figure 3.8 Output Voltage and Current Waveform at 10 kHz

CHAPTER 4. AVERAGE CURRENT MODE CONTROL DESIGN

4.1 Introduction

Peak current mode control uses peak current information to estimate the electrical charge delivered to the actuator by the switching amplifier during each switching cycle. Compared with voltage feedback control, the accuracy of the actuator's displacement output can be increased because the actuator's hysteretic behavior is reduced when charge is used as the controlled variable instead of the terminal voltage. However, peak current mode control uses a pure gain stage as the current loop compensator, which is shown in Equation (4.1) and (4.2) as $G_c(s)$:

$$T_i(s) = F_m H_e(s) G_c(s) \frac{\hat{i}_L(s)}{\hat{d}(s)} \tag{4.1}$$

$$G_c(s) = w_i \tag{4.2}$$

Since there will be no poles and zeros added to the current loop gain by current loop compensator $G_c(s)$, the poles and zeros of $T_i(s)$ will be dominated by the pole-zero configuration of the power stage inductor current to duty cycle transfer function, as shown in Figure 2.6.

From Figure 2.6, we can notice that the magnitude of the current loop gain for a switching amplifier using peak current mode control has a 20 dB per decade increasing rate at low frequencies. Since the power stage double pole appears at $f_0 = 4.38$ kHz, which means at 500 Hz, the current loop gain will be approximately 20 dB lower than the maximum current loop gain.

To ensure the current loop has good control accuracy, it is very desirable to have a current

loop loop-gain as high as possible to reduce the circuit's feedback error and increase the circuit's response speed. However, the maximum current loop loop-gain is limited by the circuit's stability requirements; the circuit will get into sub-harmonic oscillation if the current loop gain exceeds the maximum value.

For a circuit using peak current mode control, if the circuit's current loop loop-gain reaches its maximum value at its peak point, which is the power stage's LC resonant frequency, the current loop-gain magnitude will be 10 times smaller at one decade below the resonant frequency (500 Hz) and one decade above the resonant frequency (5 kHz), which means an increased feedback error and a deterioration of the switching amplifier's performance at these frequencies.

A solution to this problem is using average current mode control. Instead of using the peak current as the control variable, average current mode control uses the average charging current $\bar{i}(t)$, from Equation (3.5), we can get:

$$\frac{dS}{dt} = d' \cdot \bar{i}(t) \tag{4.3}$$

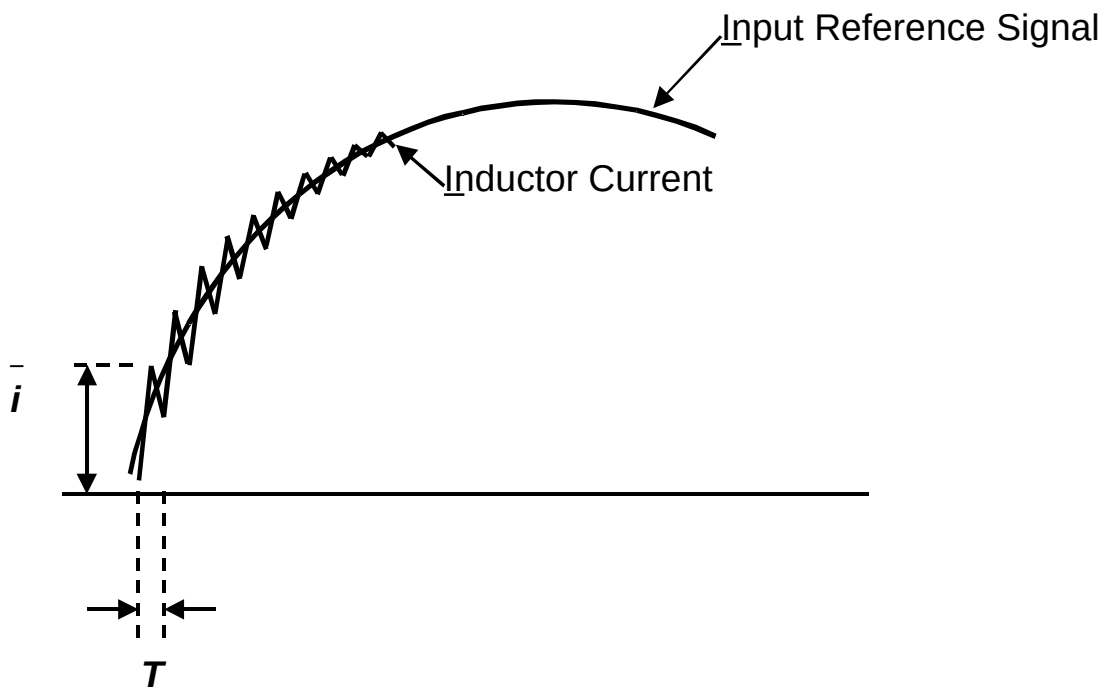

Figure 4.1 Principal of Average Current Mode Control

The principal of average current mode control is shown in Figure 4.1. Since $\bar{i}(t)$ is the actuator's average input current, the actuator's velocity output will directly follow the input reference signal.

4.2 Small Signal Modeling of Average Current Mode Control

4.2.1 Current loop design

Based on the power stage small signal analysis results given above, a current loop controller using average current mode control is designed to give an enhanced current loop gain at low frequencies. Different from peak current mode control, average current mode control has a low frequency pole at the origin in the controller, which will give a 20dB per decade decreasing rate. This decreasing rate will cancel the +20dB per decade increasing rate from

the power stage, and give a flat current loop gain before the resonant frequency, thus increasing the low frequency current loop gain. To analyze the interaction of the controller and the power stage, a small signal model for average current mode control is used and is shown in Figure 4.2 [32].

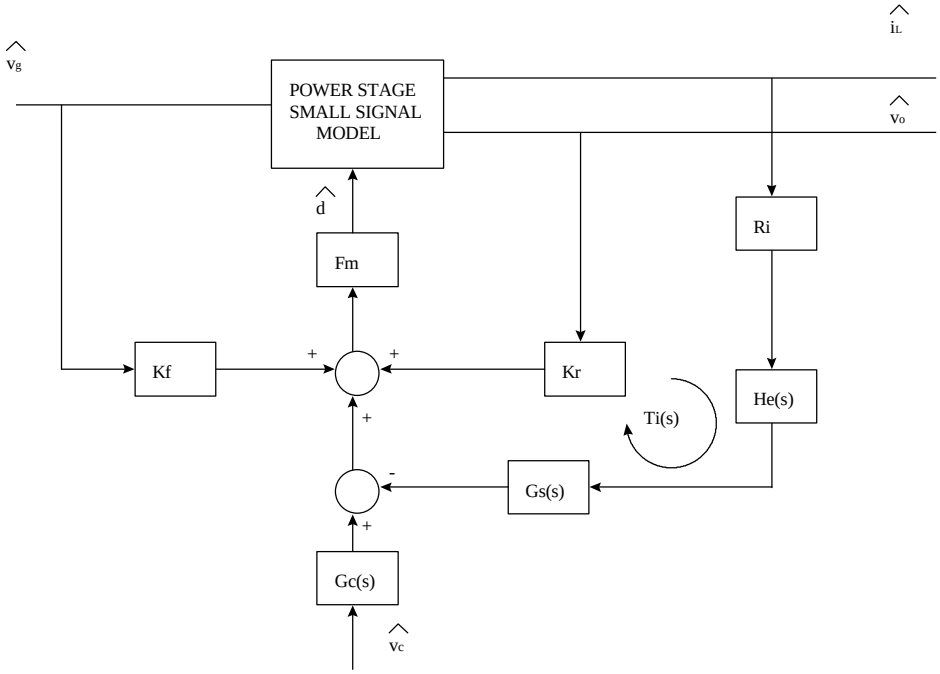

Figure 4.2 Small Signal Model of Average Current Mode Control

Where the V_g is the input voltage, F_m is the PWM gain, K_f represents the effect of line voltage perturbation on duty cycle perturbation, and K_r represents the effect of output voltage perturbation on duty cycle perturbation. R_i is the current sensor gain, $H_e(s)$ represents the sampling gain. $G_c(s)$ is the transfer function of the current loop compensator.

To implement average current mode control, a two-pole, one-zero current loop compensator is designed. The transfer function of the current loop compensator is given by [33] Equation (4.4):

$$Gc(s) = \frac{w_i \cdot (1 + \frac{s}{w_z})}{s \cdot (1 + \frac{s}{w_p})} \tag{4.4}$$

Where w_i is the current loop integrator gain, w_z is a zero in the current loop compensator, and w_p is a high frequency pole in the current loop compensator.

In this current loop compensator design, the damping factor, Q_p, is given by [33] Equation (4.5):

$$Q_p = \frac{1}{p \cdot (\frac{L \cdot F_s \cdot w_z}{Fm \cdot V_{ap} \cdot R_i \cdot w_i} - \frac{1}{2})} \tag{4.5}$$

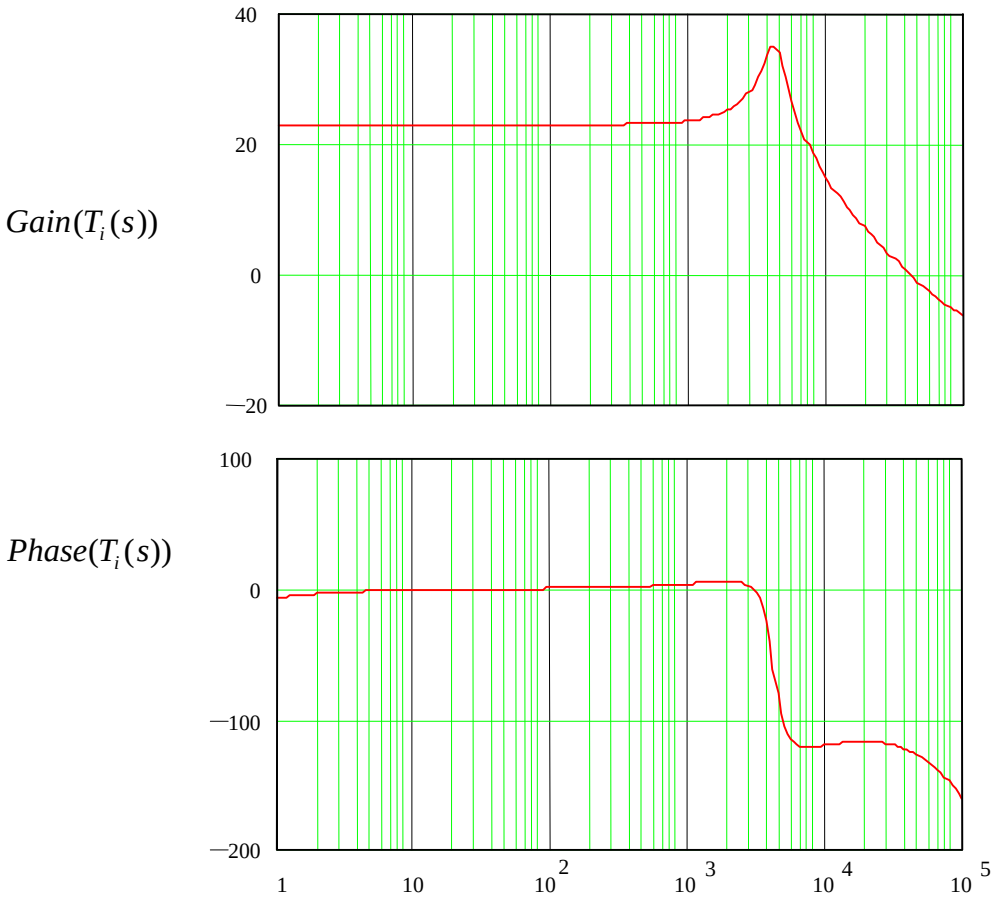

Figure 4.3 Current Loop Gain of Average Current Mode Control

By selecting the value of w_i, the current loop gain can be shaped to give the desired current loop crossover frequency, while at the same time keeping the damping factor, Q_p, less than or equal to 1. In our design, w_z is set at 0.8 times of the power stage resonant frequency, and w_p is placed at half of the switching frequency to damp the switching ripple. The small signal model analysis of the current loop with $w_i = 10^5$ is shown in Figure 4.5. We can see that with this design, the current loop gain has a crossover frequency at 50 kHz, with a phase margin around 55 degrees. The damping factor of this design is $Q_p = 0.704$.

The closed-loop control voltage to inductor current transfer function is given by:

$$Tc\_l(s) = \frac{Gc(s) \cdot Fm \cdot \frac{\hat{i}_L(s)}{\hat{d}(s)}}{1 + Ti(s)} \tag{4.6}$$

Small signal analysis of the closed-loop control voltage to inductor current transfer function is shown in Figure 4.4.

Figure. 4.4 shows that the closed-loop control voltage to inductor current transfer function can yield a very flat gain within the required frequency range. From 500 Hz to 10 kHz, The gain variation is approximately 1 dB, and the phase variation is approximately 7 degrees.

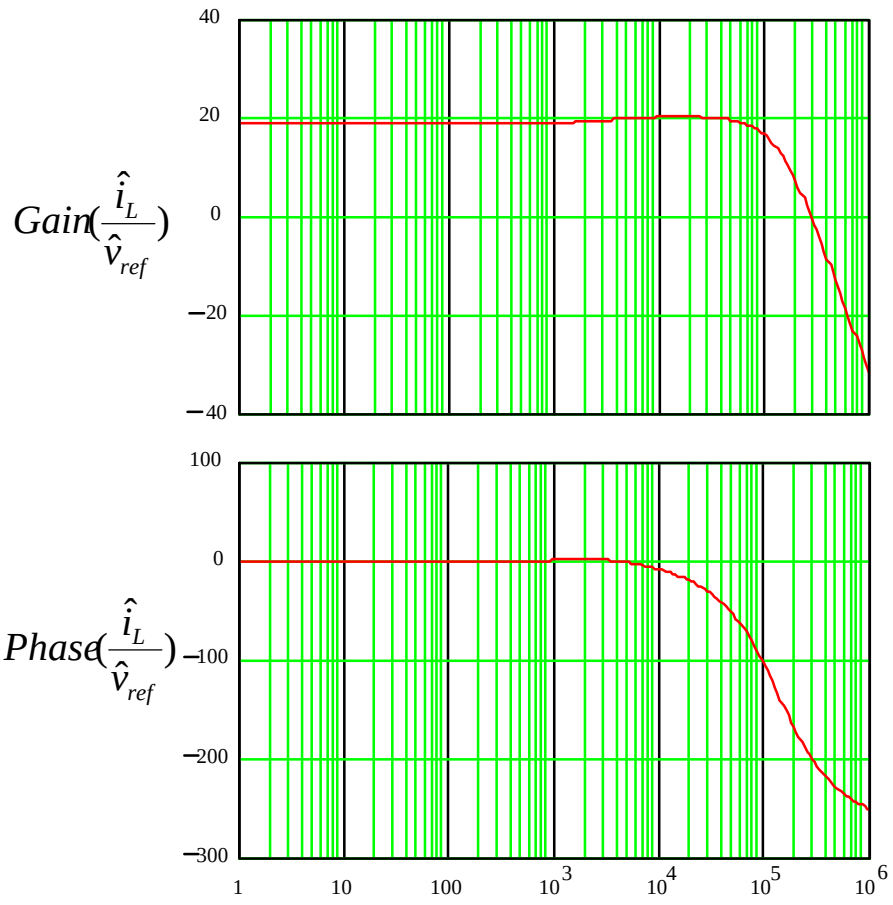

Figure 4.4 Output current to Input Signal Transfer Function Using Average Current

4.2.2 Voltage loop design

The voltage loop design is relatively easy. In our applications, voltage loop is used to regulate the output DC bias voltage, which means that the voltage feedback loop does not necessarily have to have a wide bandwidth.

A single pole compensator is designed for voltage feedback loop, and the pole is placed at the capacitor ESR zero.

The outer loop gain T2 with current loop and voltage loop closed is shown in Figure 4.5. It can be seen that the T2 has a crossover frequency of 57 kHz according to Pspice simulation.

4.3 Average Current Mode Control Design and Experiment Results

A prototype circuit is built to test the analytical results. UC 1823 PWM control IC is used to build the PWM controller with average current mode control.

Figure 4.6 shows the measurement of closed-loop input reference signal to output current transfer function. It can be seen that within the required signal bandwidth, from 500 Hz to 10 kHz, the maximum current loop gain variation is 0.7 dB, and the maximum phase variation is 7°. This result matches very well with the small signal analysis results. It can be further noted that the phase lead at 500 Hz is approximately 0°, shows the output current can follow the input reference signal with very good phase accuracy.

Figure 4.7 and Figure 4.8 show the output current waveform. The upper most trace is the output voltage waveform, the middle waveform is the reference input signal, and the bottom one shows the output current signal. Figure 4.7 is the current waveform taken at input signal frequency=500 Hz, and Figure 4.8 is taken at 10 kHz.

Again, both Figure 4.7 and Figure 4.8 show that the output current follows the input current reference signal. There is also a 90° phase shift between the output voltage signal and input current reference signal. This shows the results of current mode control.

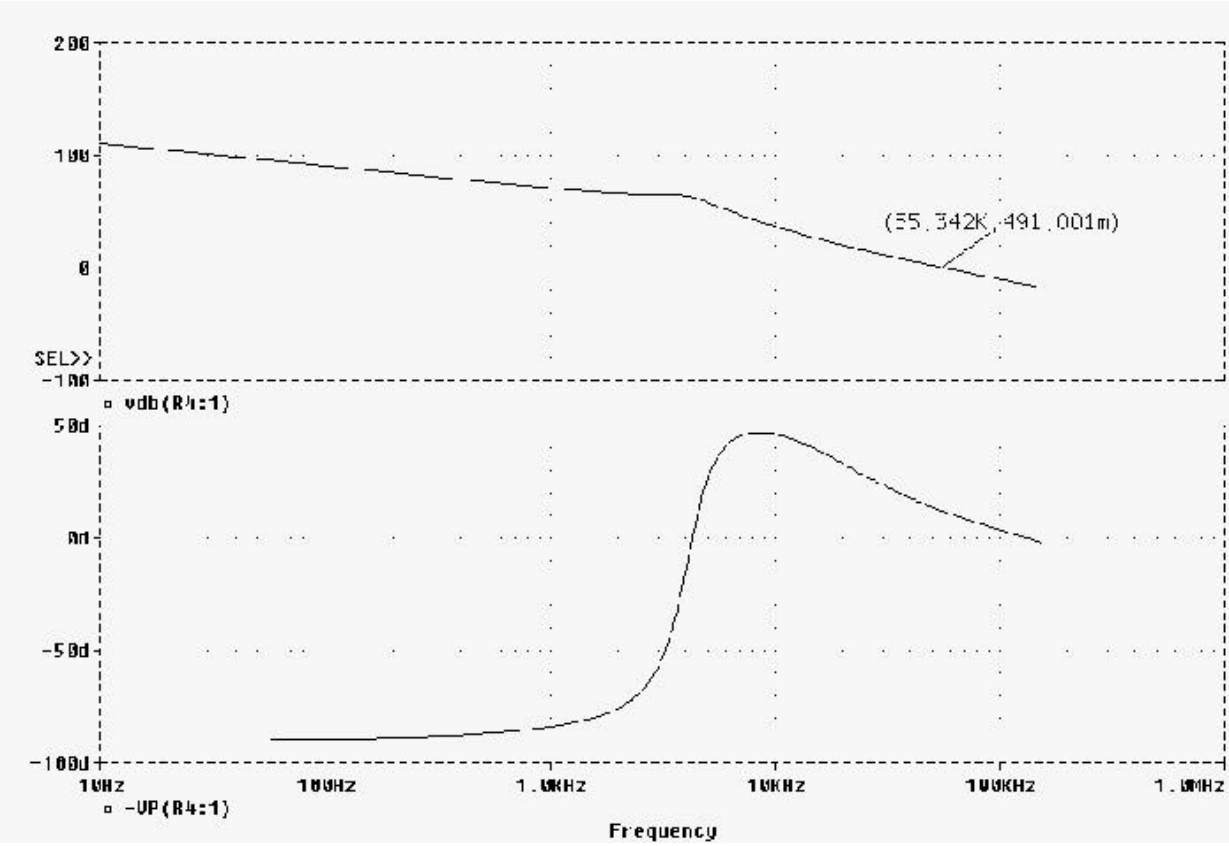

Figure 4.5 Outer Loop Gain Using Average Current Mode Control

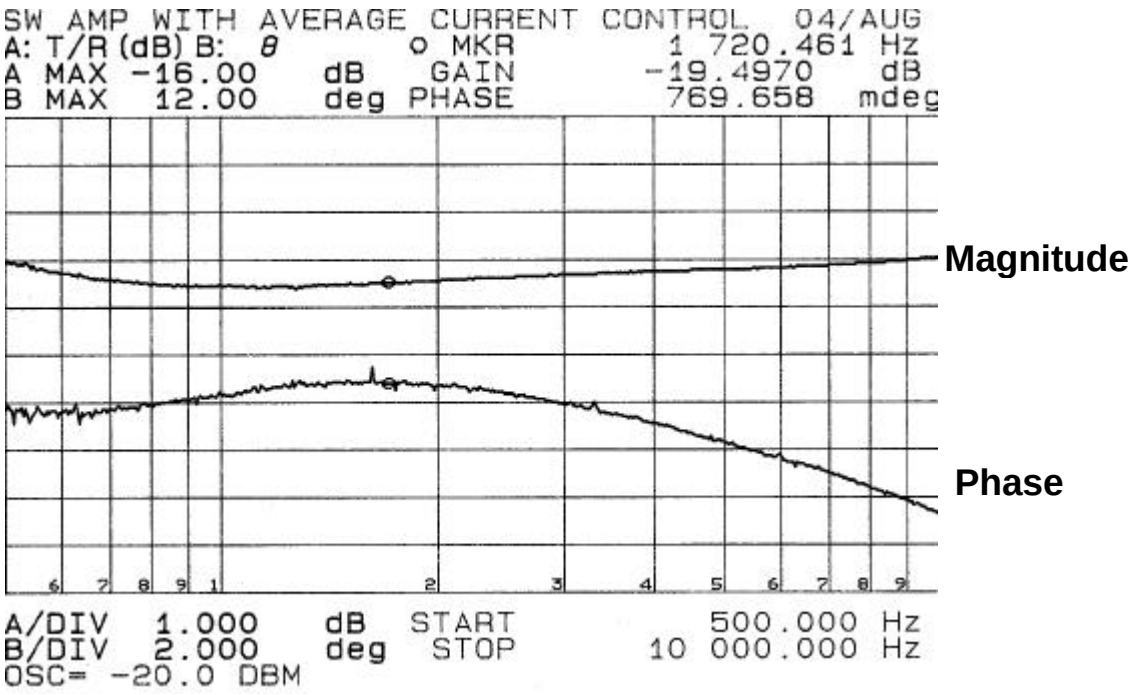

Figure 4.6 Output Current to Input Signal Transfer Function

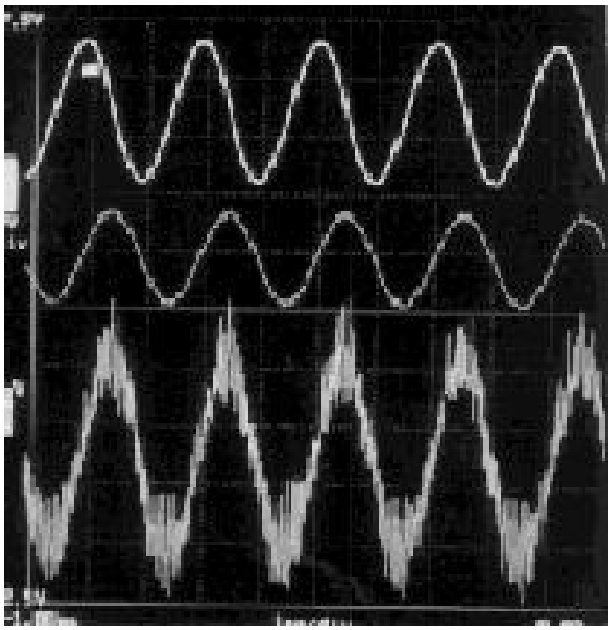

Figure 4.7 Output Current and Voltage Waveform at 500 Hz

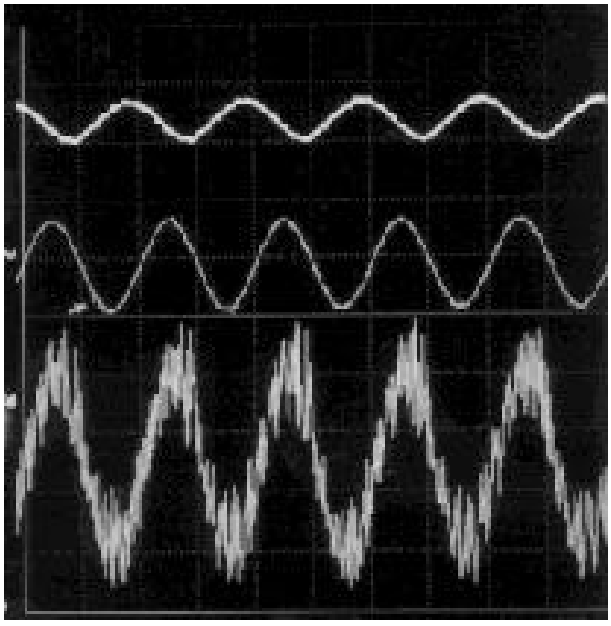

Figure 4.8 Output Voltage and Current Waveform at 10 kHz

This switching amplifier design presented in this thesis has been used in construction of an acoustic wave cancellation testbed. This testbed has done underwater tests and the experimental results show a positive outcome in the underwater acoustic wave cancellation function. Figure 4.9 shows the testbed in underwater test. Figure 4.10 and 4.11 shows the top view and bottom view of the surface mounted version of the switching amplifier.

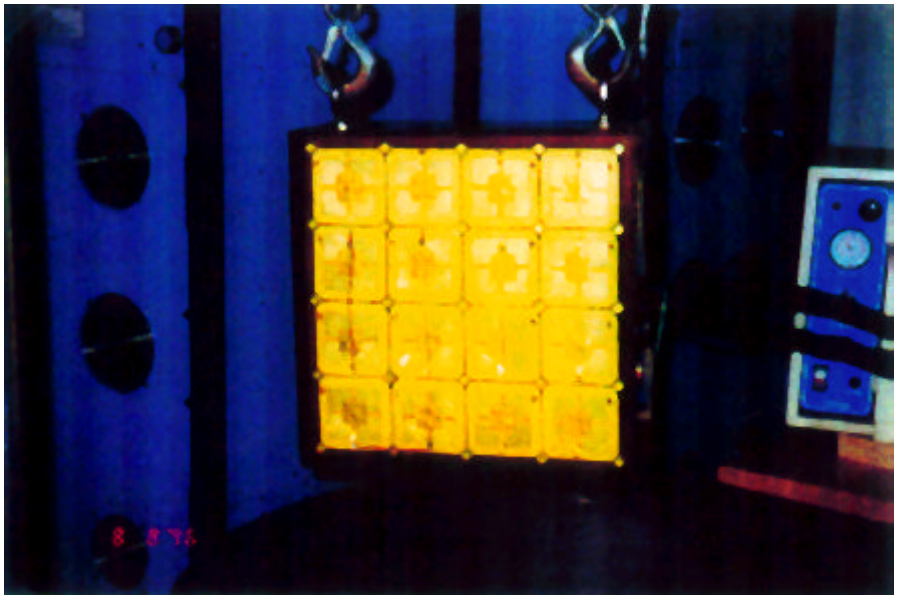

Figure 4.9 Smart Structure in Underwater Test

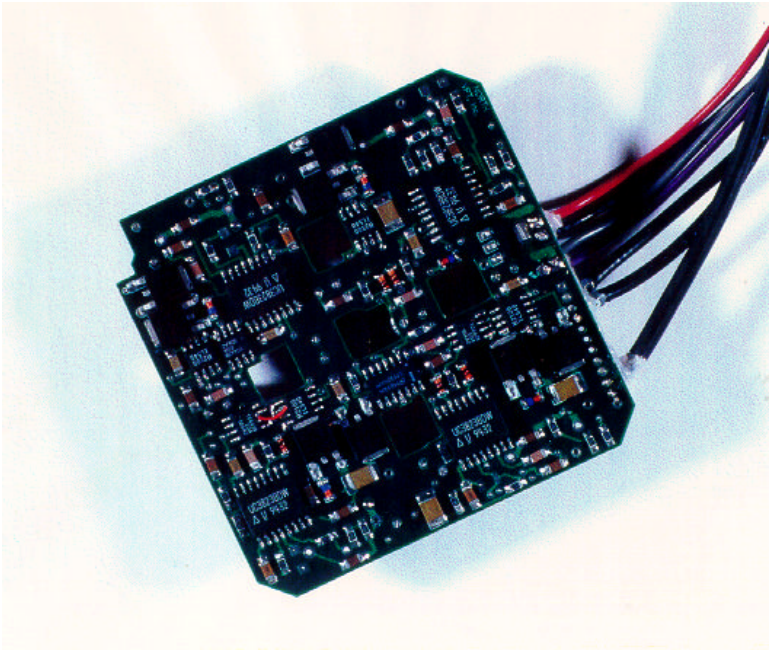

Figure 4.10 Upper View of a Surface Mounted Switching Amplifier

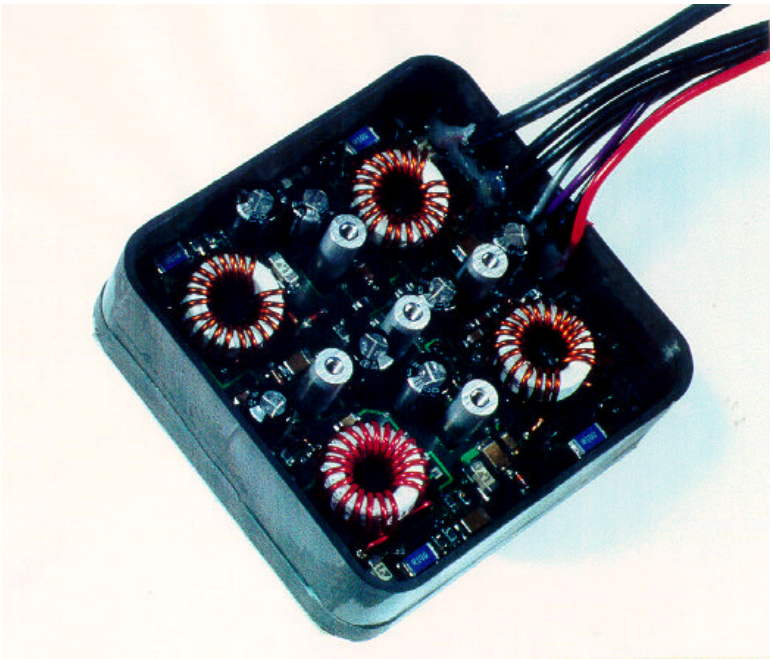

Figure 4.11 Bottom View of a Surface Mounted Switching Amplifier

Figure 4.12 shows the experimental results for piezoelectric actuators driven by a switching amplifier without current mode control. The exciting input is a sinusoidal signal, and the three traces are output voltage, output current and actuator velocity, respectively. Since current mode control is not used, the output voltage follows the input reference signal, and there is distortion in the current output due to the non-linear property of the actuator. The actuator velocity follows the output current signal which indicates that current is a better control variable than output voltage.

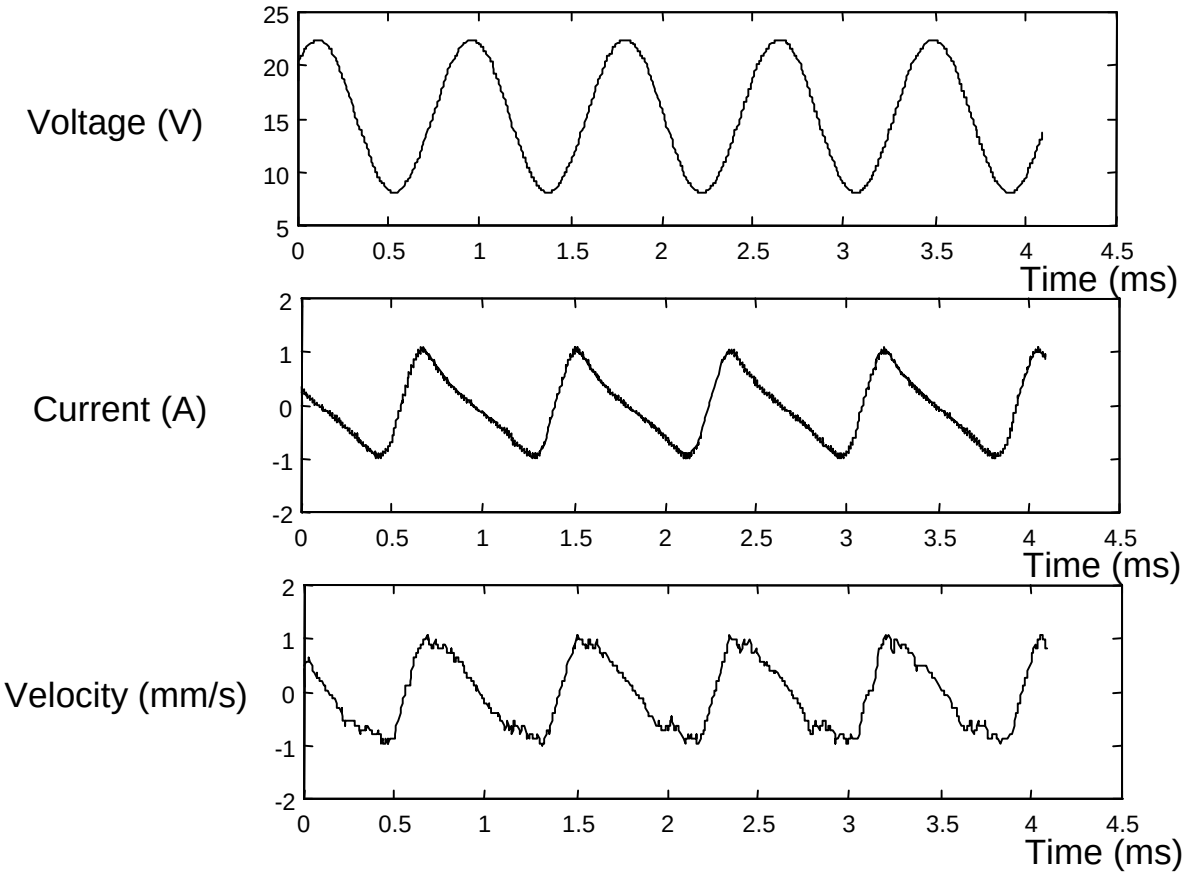

Figure 4.12 Piezoelectric Actuator Displacement Output w/o Current Mode Control

Figure 4.13 shows the experimental results for piezoelectric actuators driven by a switching amplifier with current mode control. The input reference signal is still a sinusoidal signal. Since current mode control is used, the output current follows the input reference signal,

and there is distortion in the voltage output signal due to the non-linear property of the actuator. The actuator velocity is in good agreement with the current output, which is also the reference signal.

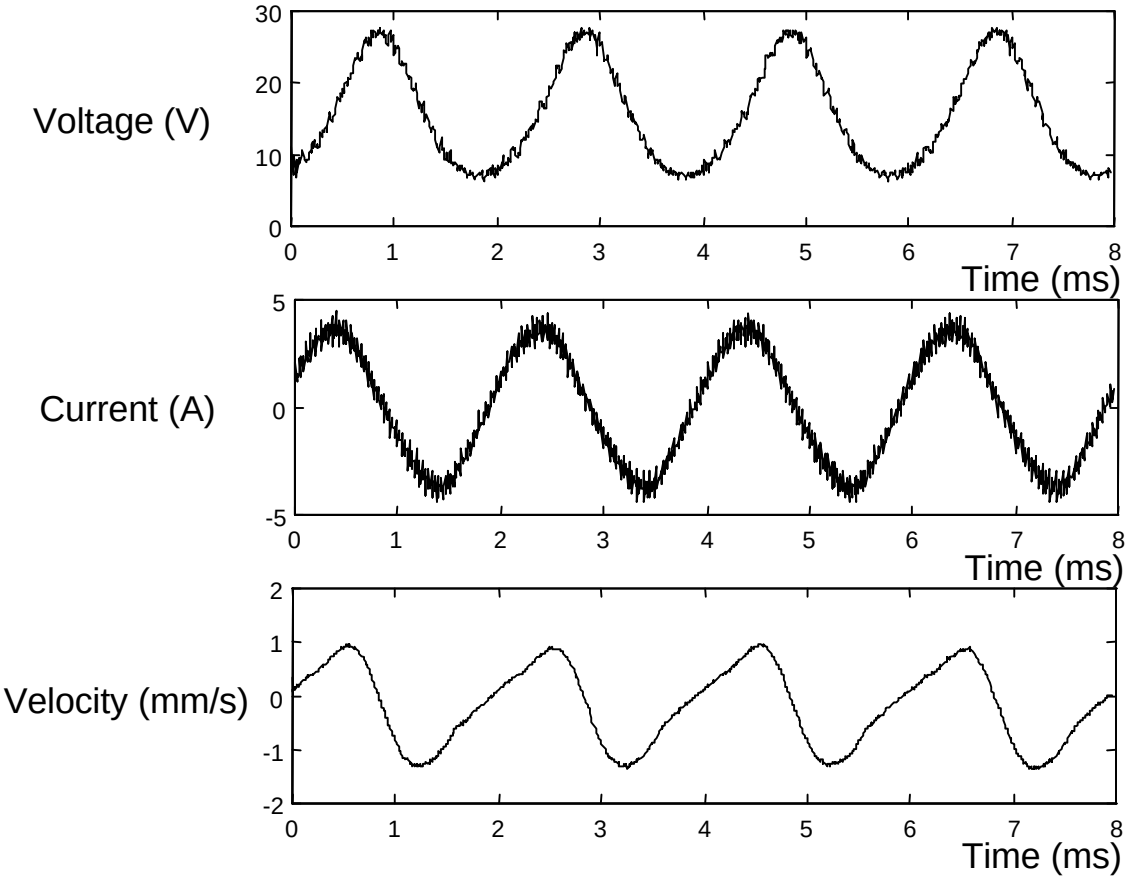

Figure 4.13 Piezoelectric Actuator Displacement Output with Current Mode Control

Figures 4.14 and 4.15 are plots that show the effectiveness of the active sonar wave cancellation. Figure 4.14 shows the sonar reflection of a submarine to an incoming sonar waves without active sonar cancellation, and Figure 4.15 shows the sonar reflection with smart material cancellation devices. At least 40 dB sonar wave attenuation can be achieved by the smart material active sonar wave cancellation devices.

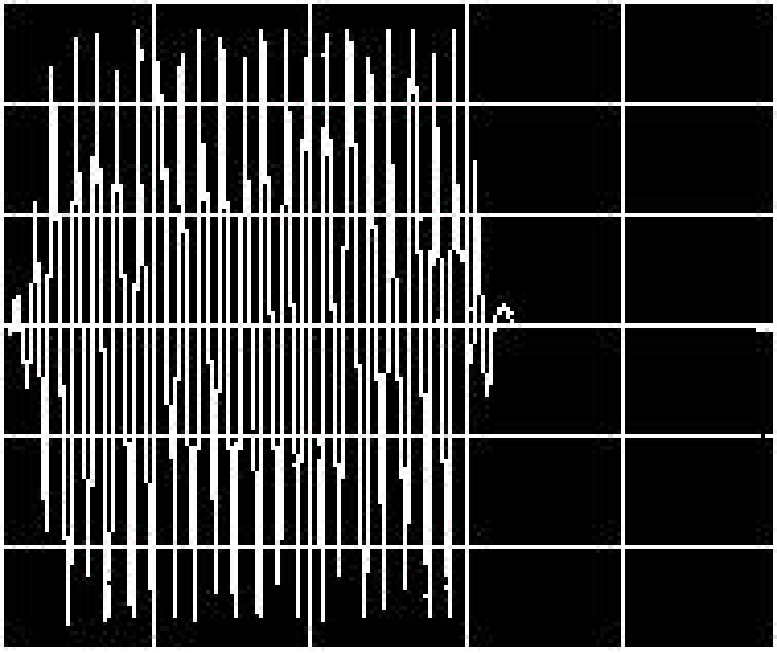

Figure 4.14 Measured Sonar Wave Without Active Sonar Wave Cancellation

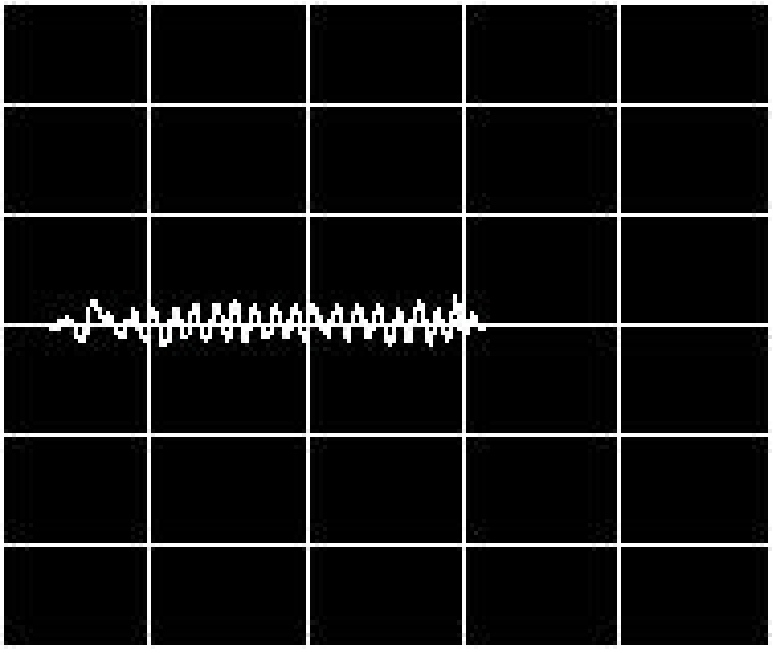

Figure 4.15 Measured Sonar Wave With Active Sonar Wave Cancellation

CHAPTER 5. CONCLUSIONS

In order to drive smart material actuators effectively and efficiently, a high frequency switching amplifier is designed and developed. Traditional linear power amplifiers are not adapted to drive reactive loads. The circulating energy from a smart material reactive load will make the linear power amplifiers extremely low efficiency and cause severe heat dissipation problems.

Conventional PWM technique can be used in the design of a high frequency switching amplifier. Besides the benefits of high efficiency and low profile, switching amplifiers provide the opportunity to use current mode control. Since the physical displacement of both piezoelectric materials and electrostrictive materials has better linearity with respect to their electrode charge rather than their terminal voltage, current mode control can provide better linearity because it reflects the charging information.

The impact of the smart material reactive load is not merely reducing the power amplifier efficiency. It also affects the current loop gain of the switching amplifier design. If there is no resistive load present, the switching amplifier will have a low current loop gain at low frequencies which tends to reduce the accuracy of the current control loop.

This thesis presents two types of the switching amplifier design. Switching amplifiers with peak current mode control is relatively easy to achieve and can provide other advantages like the switch protection feature. However, due to the fact that the current loop gain will be low when the switching amplifier is used to drive a smart material reactive load, the current control capability is limited. This will affect the closed-loop input signal to output current transfer function.

Switching amplifiers with average current mode control can provide an improved current

loop performance. The current loop compensator pole at origin can boost the current loop gain at low frequencies, thus increasing the accuracy of the current loop. A small signal analysis using the conventional PWM switch model is done together with an analysis using PSPICE simulation. These analytical results agree with the prototype circuit measurement results, and prove that average current mode control can provide the switching amplifier design with an enhanced current loop performance.

Although the use of current mode control can improve the linearity of the actuators' displacement output to their reference signal input, it cannot completely eliminate the impact of the hysteretic behavior of the smart materials, nor can it deal with the material non-linearity, especially with the electrostrictive materials. The non-linear quadratic behavior and its impact on the switching amplifier design are other open questions which deserve further investigation in the future.

REFERENCES

[1] T. Takagi, "A Perspective of the Intelligent Materials," *Proceedings of the first ICIM*, Vol. 1, pp. 3-8, 1992.

[2] G. Beck and P.F. Gobin, "The Research on Intelligent Materials Developed in Relations with the National Center for Scientific Research (CNRS)-France," *Proceedings of the first ICIM*, Vol. 1, pp. 9-22, 1992.

[3] W.B. Spillman Jr. et al., "Smart Materials and structures: What Are They," *Smart Mater. Struct.* , Vol. 5, pp. 247-254, 1996.

[4] D. Damjanovic and R. E. Newnham, " Electrostrictive and Piezoelectric Materials for Actuator Applications," *J. of Intell. Mater. Syst. And Struct.*, Vol. 3, pp. 190-207, 1992.

[5] Gary H. Blackwood and Mark A. Ealey, "Electrostrictive Behavior in Lead Magnesium Niobate (PMN) Actuators. Part I: Materials Perspective," *Smart Mater. Struct.*, Vol. 2, pp. 124-133, 1993.

[6] T. Tanaka "Piezoelectric Devices in Japan," *Piezoelectricity*, Rosen C.Z et al. ed., pp. 289-309, New York, 1992.

[7] D. Berlincourt, "Current Developments in Piezoelectric Applications of Ferroelectrics," *Ferroelectrics*, Vol. 10, pp. 111-119, 1976.

[8] M. R. Keeling, "Inkjet Printing," *Piezoelectricity*, Rosen C.Z et al. ed., pp. 339-346, New York, 1992.

[9] Shinsei Kogyo Co., "Ultrasonic Wave Motor, the First Actuator Incorporating Ceramics Technology," *Piezoelectricity*, Rosen C.Z et al ed., pp.381-383, New York, 1992.

[10] Chih-yi Lin, "Design and Analysis of Piezoelectric Transformer Converters," *PhD Dissertation*, Virginia Polytechnic Institute and State University, 1997.

[11] B. Jaffe, *Piezoelectric Ceramics*, New York, Academic Press, 1971, pp. 1-5.

[12] L. E. Cross and K. H. Hardtl, "Ferroelectrics," *Piezoelectricity*, Rosen C.Z et al. ed., pp.2-31, New York, 1992.

[13] Z. L. Wang and Z. C. Kang, *Functional and Smart Materials-Structural Evolution and Structure Analysis*, Atlanta, Plenum Press, 1998, pp. 93-149.

[14] K. Uchino, "Electrostrictive Actuators: Materials and Applications," *Piezoelectricity*, Rosen C.Z et al. ed., pp. 331-336, New York, 1992.

[15] David J. Warkentin and Edward F. Crawley, "Power Flow and Amplifier Design for Piezoelectric Actuators in Intelligent Structures," *SPIE*, Vol. 2190, pp. 283-294, 1994.

[16] ACX Inc., *ACX 1224/5 QuickPack Power Amplifier Catalog*, Cambridge, 1994.

[17] Standards Committee of the IEEE Ultrasonics, Ferroelectrics, and Frequency Control Society. "An American National Standard: IEEE Standard on Piezoelectricity: The Institute of Electrical and Electronics Engineers," *ANSI/IEEE Std.* 176-1987. New York, 1987.

[18] APEX Microtechnology Corp. *APEX Data Book*, Vol. 6, p. B5, 1993.

[19] C. Newcomb and I. Flnn, "Improving the Linearity of Piezoelectric Ceramic Actuators," *Electronics Letters*, Vol. 18. (11), pp. 442-444,1982.

[20] R. H. Comstock, "Charge Control of Piezoelectric Actuators to Reduce Hysteresis Effects," *US Patent, 4,263,527*, 1981.

[21] John A. Main, David V. Newton, Lloyd Massengill and Ephrahim Garcia, "Efficient Power Amplifiers for Piezoelectric Applications," *Smart Mater. Struct.*, Vol. 5, pp.766-775, 1996.

[22] G. A. Zvonar, J. Luan F.C. Lee, D.K. Lindner, S.Kelly, D. Sable and T. Schelling, "High-Frequency Switching Amplifiers for Electrostrictive Actuators," *Proceeding of SPIE's 1996 North American Symposium on Smart Structures and Materials: Industrial and Commercial Applications of Smart Structures Technologies*, C. Robert Crowe; Ed., Vol. 2721, San Diego, CA, February, 1996, pp. 465-475.

[23] Dan Sable, Troy Schelling, D. K. Lindner, F. C. Lee, J. Luan and G. A. Zvonar, " Power Supplies for Piezoelectric Actuators," *Final Report*, Virginia Polytechnic Institute and State University, 1997.

[24] J. Luan and F. C. Lee, "Design of a High Frequency Switching Amplifier for Smart Material Actuators with Improved Current Mode Control," *PESC 98*, Vol. 1, pp. 59-64, Fukuoka, May 1998.

[25] Vorperian V., "Simplified Analysis of PWM Converters Using the Model of the PWM Switch Part I: Continuous Conduction Mode," *Modeling, Analysis, and Design of PWM Converters*, VPEC publication Series, Vol. 2, pp. 87-95.

[26] Raymond B. Ridley, Bo H. Cho and Fred C. Y. Lee, "Analysis and Interpretation of Loop Gains of Multiloop-Controlled Switching Regulators," *IEEE Transactions on Power Electronics*, Vol. 3, pp. 489-498.

[27] Motorola, *Semiconductor Technical Data*, Vol.6, pp. 72-78.

[28] Micromentals, *Power Conversion Line Filter Applications*, Catalog 4.

[29] M. Goldfarb and N. Celanovic, "A Lumped Parameter Electromechanical Model for Describing the Nonlinear Behavior of Piezoelectric Actuators," *Transactions of the ASME*, Vol. 119(3), pp. 478-485, 1997.

[30] M. Goldfarb and N. Celanovic, "Modelling Piezoelectric Stack Actuators for Control of Micromanipulation," *IEEE Control Systems Magazine*, Vol 17(3), pp. 69-79, 1997.

[31] J. Main, E. Garcia. and D. Newton., "Precision Position Control of Piezoelectric Stack Actuators," *J. Guid. Control Dyn.* Vol. 18(6), pp. 112-117, 1995.

[32] F. C. Lee, B. H. Cho, *Course I-Control Design: Lecture Notes*, VPEC Power Electronics Professional Seminar, 1991.

[33] Wei Tang, " Average Current-Mode Control and Charge Control for PWM Converters," *Ph.D. Dissertation*, Virginia Polytechnic Institute and State University, 1994.

APPENDIX A

From Equation (1.1), we can get the first order linearized approximation as rewritten in equation (A.1).

$$S = s^E T + dE \tag{A.1}$$

Where

S	strain
s^E	elastic compliance at constant total field
T	stress
d	piezoelectric constant

This is also the most widely accepted piezoelectric ceramic behavior given by the committee of the IEEE Ultrasonics, Ferroelectrics and Frequency Control Society. Since the electric field E is the applied voltage V divided by the piezoelectric/electrostrictive material thickness l.

$$E = \frac{V}{l} \tag{A.2}$$

Substitute Equation (A.2) into Equation (A.1), yields

$$S = s^E T + d\frac{V_{out}}{l} \tag{A.3}$$

where

V_{out}	applied voltage

l material thickness

For given material, s^E, T, d and l are constants. With applied AC voltage

$$V_{out} = |V_{out}| \cdot \sin(2pft + w_0) \tag{A.4}$$

The actuator velocity output $\frac{dS}{dt}$ is proportional to the input signal frequency

$$\frac{dS}{dt} = \frac{2pd}{l} \cdot f \cdot |V_{out}| \cdot \cos(2pft + w_0) \tag{A.5}$$

If the power amplifier has a frequency response as shown in Figure 1.6, which is shown in Equation (A.6)

$$\frac{|V_{out}|}{|V_{ref}|} = \frac{1}{f} \tag{A.6}$$

This translates the actuator velocity output $\frac{dS}{dt}$ with respect to the DSP unit reference signal V_{ref} as:

$$\frac{dS}{dt} = \frac{2pd}{l} \cdot |V_{ref}| \cdot \cos(2pft + w_0) \tag{A.7}$$

So we can get constant actuator velocity output with the specified frequency response.

VITA

JIYUAN LUAN

Born in Jinan, Shandong Province, P. R. China, the author received his Bachelor of Science degree in electrical engineering in Tsinghua University, Beijing, China, in 1988. He received his Bachelor of Science degree in medical science in Beijing Medical University, Beijing, China, in 1991. Upon completion of his medical degree, the author assumed a teacher's position in the Department of Electrical Engineering in Tsinghua University, Beijing, China. The author joined Virginia Power Electronics Center (VPEC) of Virginia Tech in 1995, where he worked as a graduate research assistant, laboratory supervisor and computer system administrator respectively. His research interests at VPEC concentrated on high-frequency switching amplifier design and high frequency DC-DC converters.